Sensitivity analysis and passive control of cylinder flow

OLIVIER MARQUET, DENIS SIPP
AND LAURENT JACQUIN

ONERA/DAFE, 8 rue des Vertugadins, 92190 Meudon, France

A general theoretical formalism is developed to assess how base-flow modifications may alter the stability properties of flows studied in a global approach of linear stability theory. It also comprises a systematic approach to the passive control of globally unstable flows by the use of small control devices. This formalism is based on a sensitivity analysis of any global eigenvalue to base-flow modifications. The base-flow modifications investigated are either arbitrary or specific ones induced by a steady force. This leads to a definition of the so-called sensitivity to base-flow modifications and sensitivity to a steady force. These sensitivity analyses are applied to the unstable global modes responsible for the onset of vortex shedding in the wake of a cylinder for Reynolds numbers in the range $47 \leqslant Re \leqslant 80$. First, it is demonstrated how the sensitivity to arbitrary base-flow modifications may be used to identify regions and properties of the base flow that contribute to the onset of vortex shedding. Secondly, the sensitivity to a steady force determines the regions of the flow where a steady force acting on the base flow stabilizes the unstable global modes. Upon modelling the presence of a control device by a steady force acting on the base flow, these predictions are then extensively compared with the experimental results of Strykowski & Sreenivasan (*J. Fluid Mech.*, vol. 218, 1990, p. 71). A physical interpretation of the suppression of vortex shedding by use of a control cylinder is proposed in the light of the sensitivity analysis.

1. Introduction

Many studies have been dedicated to understanding the dynamics of a cylinder flow for various values of the Reynolds number. In particular it is well known that at a critical Reynolds number $Re_c \approx 47$ the flow experiences a Hopf bifurcation from a steady symmetric state towards a time-periodic non-symmetric state (Provansal, Mathis & Boyer 1987; Sreenivasan, Strykowski & Olinger 1987; Noack & Eckelmann 1994). A global instability has clearly been identified as responsible for the onset of the vortex shedding process (Jackson 1987; Zebib 1987) but substantial work is still devoted to understanding the mechanism for selecting its frequency (Pier 2002; Barkley 2006; Sipp & Lebedev 2007).

Control of vortex shedding has also received much attention and various passive and active control techniques have been tested on this flow both experimentally and numerically. Concerning passive control, Strykowski & Sreenivasan (1990) have experimentally investigated how a small control cylinder suitably placed in the wake of the main cylinder alters the vortex shedding. For various diameter ratios of the two cylinders they determined the regions of the flow where the placement of the control

cylinder leads to a complete suppression of the phenomenon over a specific range of Reynolds numbers. They also provided experimental evidence linking vortex shedding to the onset of a global instability, and the effect of an appropriately positioned control cylinder on damping of this instability. The same optimal positions were found by Kim & Chang (1995) and Mittal & Raghuvanshi (2001), from direct numerical simulations based on finite element formulations, and by Morzynski, Afanasiev & Thiele (1999), who performed a global stability analysis of cylinder flow in the presence of a small control cylinder. This study in particular confirmed the role of the control cylinder in damping the global instability responsible for the shedding process. All these approaches successfully determined the optimal placement of a control cylinder to suppress the vortex shedding, but required that various locations of the control cylinder be tested and either experimental measurements, direct numerical simulations or global stability analyses be carried out in each case. This paper aims to develop a more systematic approach for the passive control of vortex shedding, relying on a theoretical analysis to predict where the control cylinder should be placed to damp the global instability.

The present analysis is closely related to recent studies which focused, in a global approach of linear stability theory, on the determination of the *wavemaker region*, i.e. the region of the flow where physical mechanisms giving rise to a self-sustained flow oscillation are active. Chomaz (2005) suggested computing not only the leading direct global mode, which describes the self-sustained flow oscillation, but also the associated adjoint global mode. By studying the Ginzburg–Landau model equation, he showed that the wavemaker region can be identified as the overlapping region between the direct and adjoint global eigenvectors. More recently Giannetti & Luchini (2007) have identified the wavemaker region in the case of two-dimensional open flows. Their approach relies on a structural sensitivity analysis of the two-dimensional linearized Navier–Stokes operator. It consists of assessing the variations of the eigenvalue induced by generic structural modifications of this operator. They proposed modelling the feedback mechanisms triggering the global instability by a specific structural modification of the perturbation operator: a local force proportional to the perturbation velocity acting as a momentum source in the perturbation equations. They identified the wavemaker region as the region where such a localized feedback induces strong variations of the leading eigenvalue, and showed that it is included in the overlapping region of the leading direct and adjoint global mode velocities. Finally, they noticed that the wavemaker region is similar to the region where the placement of a control cylinder suppresses the vortex shedding in the experiments of Strykowski & Sreenivasan (1990). This suggests that the presence of a small control cylinder modifies the flow stability because it induces a structural modification of the equations at the perturbation level. However the presence of a control cylinder also modifies the base flow on which the perturbations evolve and thus might alter their dynamics. This effect has not been taken into account by Giannetti & Luchini (2007).

The present paper puts emphasis on the role of the base flow in the perturbation dynamics, by quantifying how stability properties are altered by base-flow modifications. A similar approach has been developed in the case of parallel flows by Bottaro, Corbett & Luchini (2003) in a local temporal framework and by Hwang & Choi (2006) in a local spatial framework. The so-called *sensitivity to base-flow modifications* concept is defined here in a global framework. In particular arbitrary base-flow modifications are used to identify the regions and properties of the base flow that contribute strongly to the instability dynamics. A new sensitivity analysis called sensitivity to a steady force is also developed, in which specific base-flow

modifications induced by a steady force acting on the base flow are considered. Following the precursor work of Hill (1992), this leads to a theoretical approach to the control of vortex shedding by means of a small control cylinder which relies on the modelling of the control cylinder by a steady local force at the base-flow level and not at the perturbation level as in Giannetti & Luchini (2007).

The paper is organized as follows. The theoretical framework is presented in §2. It includes the description of the linear flow dynamics in a global framework, the presentation of the sensitivity to arbitrary base-flow modifications based on the determination of gradients through adjoint methods, and the presentation of the sensitivity to a steady force. Since these concepts are not restricted to cylinder flow, the analysis is derived for a general unspecified open flow. We then focus on cylinder flow and on its passive control via a small cylinder, which is taken as an application of these techniques. First, the flow around the main cylinder alone is described in §3, together with the numerical procedure used throughout the study. The global stability analysis identifies the leading global mode and the two sensitivity analyses are then performed on that global mode. Section 4 describes their results in a general sense, i.e. by considering arbitrary modifications of the base flow and arbitrary steady forces. Passive control by means of a small cylinder is specifically investigated in §5, in which the sensitivity analysis to a steady force is particularized by modelling the presence of the control cylinder by a local steady force. The effect of all possible positions of the control cylinder on vortex shedding is theoretically predicted, and the results are compared to the experimental measurements of Strykowski & Sreenivasan (1990). Finally, a more physical interpretation of these results is proposed in §6 by applying the sensitivity analysis to base-flow modifications to the specific base-flow modifications induced by the presence of the control cylinder.

2. Theoretical framework

This section is devoted to a description of the theoretical framework used in our study. As some new concepts are introduced here whose application is general and not restricted to cylinder flow, the flow configuration is deliberately kept unspecified.

We therefore consider the two-dimensional open flow of a viscous fluid in a closed domain for which we assume that suitable inlet, outlet and lateral boundaries and solid walls have been defined. The fluid motion is then described by the velocity and pressure fields $(\boldsymbol{u}, p)$, which are supposed to obey the unsteady incompressible Navier–Stokes equations:

$$\partial_t \boldsymbol{u} + \nabla \boldsymbol{u} \cdot \boldsymbol{u} + \nabla p - Re^{-1} \nabla^2 \boldsymbol{u} = \boldsymbol{f}, \quad \nabla \cdot \boldsymbol{u} = 0, \tag{2.1}$$

where the action of a body force $\boldsymbol{f}$ has been taken into account. We use a reference length L of the configuration and the inlet velocity U_∞ (assumed uniform) as length and velocity scales, so that the Reynolds number of the problem is $Re = U_\infty L / \nu$, with ν the kinematic viscosity of the fluid. The velocity components in the streamwise x and cross-stream y directions are denoted $\boldsymbol{u} = (u, v)^T$ where ^{T} designates the transpose. The nonlinear terms are written using the tensorial notation, i.e. $(\nabla \boldsymbol{u})_{i,j} = \partial_{x_j} u_i$. The Navier–Stokes equations (2.1) are completed with the following boundary conditions: $\boldsymbol{u} = (1, 0)$ at the inlet, an outflow boundary condition $p\boldsymbol{n} - Re^{-1}(\nabla \boldsymbol{u}) \cdot \boldsymbol{n} = \boldsymbol{0}$ at the outlet, symmetric boundary conditions on the lateral boundaries and no-slip conditions $\boldsymbol{u} = \boldsymbol{0}$ on the solid walls.

We assume that the boundary conditions and the value of the Reynolds number allow the existence of a steady solution $(\boldsymbol{U}, P)$ of the Navier–Stokes equation. In

order to account for the stability of this solution, the flow (u, p) is described as a superposition of (U, P) taken as the base flow, and of an infinitesimal unsteady perturbation (u', p'). Furthermore, in our analysis the body force f is assumed to be steady and to act only on the base flow, i.e. $f(x, y, t) = F(x, y) = (F_x, F_y)^T$. The steady incompressible Navier–Stokes equations governing the base flow are therefore

$$\nabla U \cdot U + \nabla P - Re^{-1} \nabla^2 U = F, \quad \nabla \cdot U = 0, \qquad (2.2)$$

with the same boundary conditions as for the Navier–Stokes equations. The perturbation is sought in the form of normal modes $(u'(x, y, t), p') = (\hat{u}, \hat{p})(x, y) \exp[\sigma t]$, where σ is a complex eigenvalue associated with the complex fields $(\hat{u}, \hat{p})$. The unsteady Navier–Stokes equations linearized around the base flow (U, P) may then be written as

$$\sigma \hat{u} + \nabla \hat{u} \cdot U + \nabla U \cdot \hat{u} = -\nabla \hat{p} + Re^{-1} \nabla^2 \hat{u}, \quad \nabla \cdot \hat{u} = 0, \qquad (2.3)$$

the associated boundary conditions consisting of the Dirichlet condition $\hat{u} = 0$ at the inlet and the same boundary conditions as for the Navier–Stokes equations for the other boundaries. In this equation, the base flow is seen to influence the perturbations via the velocity only, namely by a term for downstream transport of the perturbations $(\nabla \hat{u} \cdot U)$ and by a term related to production of perturbations $(\nabla U \cdot \hat{u})$.

Solutions $(\hat{u}, \hat{p})$ of the eigenproblem given by (2.3) together with its associated boundary conditions constitute the set of linear global modes of the stability problem. Each mode is associated with a complex eigenvalue $\sigma = \lambda + i\omega$, whose real part λ is the growth rate of the mode and whose imaginary part ω is its frequency. We hereafter consider a particular eigenvalue σ. According to equations (2.3), it is a function of the base-flow velocity, i.e. $\sigma(U)$. Moreover according to equations (2.2), the velocity field U is a function of the steady force F, i.e. $U(F)$. As a consequence the eigenvalue σ is also a function of F, that is $\sigma(U(F)) = \sigma(F)$. Thus it appears that variations of a given eigenvalue $\delta\sigma$ may be investigated with respect to small variations of:
  (i) the base flow δU if σ is viewed as a function of U;
  (ii) the steady force δF if σ is viewed as a function of F.
  The former case defines the analysis of sensitivity to base-flow modifications, and the latter, the analysis of sensitivity to a steady force.

2.1. *Sensitivity to base-flow modifications*

The sensitivity analysis of a given eigenvalue to arbitrary base-flow modifications is first considered. Note that this is an extension to the global framework of a concept that was originally developed by Bottaro *et al.* (2003) in a local framework. Let us consider a particular eigenpair $(\sigma; \hat{u}, \hat{p})$ associated with the base flow (U, P), i.e. $(\sigma; \hat{u}, \hat{p})$ is a solution of the eigenproblem given by (2.3) together with its associated boundary conditions. We investigate the variations of the complex eigenvalue $\delta\sigma$ with respect to small-amplitude base-flow modifications δU. Here it is worth emphasizing that these modifications are generic since they are chosen with an arbitrary form, i.e. we do not require $U + \delta U$ to be a steady solution of the base-flow equations (2.2). The variations $\delta\sigma$ and δU are then formally linked through

$$\delta\sigma = (\nabla_U \sigma, \delta U). \qquad (2.4)$$

In this relationship, the gradient $\nabla_U \sigma$ defines the so-called sensitivity to base-flow modifications, which is a complex vector field since $\delta\sigma$ is complex and δU is real. This expression involves the inner product of two complex vector fields u_A and u_B which is defined by $(u_A, u_B) = \int_\Omega (u_A^* \cdot u_B) \, d\Omega$, * denoting the conjugate of a complex quantity.

Variations of the growth rate $\delta\lambda$ and frequency $\delta\omega$ may similarly be expressed as

$$\delta\lambda = (\nabla_U \lambda, \boldsymbol{\delta U}), \quad \delta\omega = (\nabla_U \omega, \boldsymbol{\delta U}), \tag{2.5}$$

thereby defining the growth rate and frequency sensitivities $\nabla_U \lambda$ and $\nabla_U \omega$. From (2.4), these real quantities are seen to be linked to $\nabla_U \sigma$ via $\nabla_U \lambda = \mathrm{Re}\{\nabla_U \sigma\}$ and $\nabla_U \omega = -\mathrm{Im}\{\nabla_U \sigma\}$.

In order to derive the sensitivity $\nabla_U \sigma$ associated with the base flow U, we use in this study a Lagrangian-based approach (Gunzburger 1997) that is classically used in optimal flow control problems (see for instance Airiau *et al.* 2003). Details of the computations are given in Appendix A and show that

$$\nabla_U \sigma = \underbrace{-(\nabla\hat{\boldsymbol{u}})^H \cdot \hat{\boldsymbol{u}}^+}_{\nabla_{U,T}\,\sigma} + \underbrace{\nabla\hat{\boldsymbol{u}}^+ \cdot \hat{\boldsymbol{u}}^*}_{\nabla_{U,P}\,\sigma}. \tag{2.6}$$

Here, ^{H} designates the transconjugate and $(\hat{\boldsymbol{u}}^+, \hat{p}^+)$ is the adjoint global mode associated with $(\hat{\boldsymbol{u}}, \hat{p})$ which satisfies

$$\sigma^* \hat{\boldsymbol{u}}^+ - \nabla\hat{\boldsymbol{u}}^+ \cdot \boldsymbol{U} + (\nabla\boldsymbol{U})^T \cdot \hat{\boldsymbol{u}}^+ = -\nabla\hat{p}^+ + Re^{-1}\nabla^2\,\hat{\boldsymbol{u}}^+, \quad \nabla\cdot\hat{\boldsymbol{u}}^+ = 0, \tag{2.7}$$

with $\hat{\boldsymbol{u}}^+ = \boldsymbol{0}$ at the inlet and on the solid walls and symmetrical boundary conditions on the lateral boundaries. The boundary conditions at the outlet are given in Appendix A. Note that the following condition is used to normalize the adjoint:

$$(\hat{\boldsymbol{u}}^+, \hat{\boldsymbol{u}}) = 1. \tag{2.8}$$

Comparison of the direct (2.3) and adjoint (2.7) eigenproblems shows that the transport terms appear with opposite signs, i.e. the adjoint perturbations are convected upstream while the direct ones are convected downstream, and that the production term appears in (2.7) with a transpose in the base-flow velocity gradient.

The specific form chosen for equation (2.6) allows further physical interpretation of the sensitivity $\nabla_U \sigma$ since the two terms on its right-hand side stem from two different physical origins. Bearing in mind the structure of the stability eigenproblem (2.3), it can indeed be shown (see the details of the derivation in Appendix A.2) that the first term, denoted $\nabla_{U,T}\,\sigma$, originates from the term for transport of perturbations by the base-flow $\nabla\hat{\boldsymbol{u}}\cdot\boldsymbol{U}$ while the second, denoted $\nabla_{U,P}\,\sigma$, originates from the term for production of perturbations by the base flow $\nabla\boldsymbol{U}\cdot\hat{\boldsymbol{u}}$. We therefore respectively call the two sensitivities $\nabla_{U,T}\,\sigma$ and $\nabla_{U,P}\,\sigma$ sensitivity to modifications of the transport and sensitivity to modifications of the production.

From a physical point of view, $\nabla_U \sigma$ allows us to determine the region of the flow where the eigenvalue σ is most sensitive to modifications of the base flow. The properties of the base flow in this region are therefore crucial in determining the global eigenvalue. The analysis of $\nabla_{U,T}\,\sigma$ and $\nabla_{U,P}\,\sigma$ further indicates whether transport or production processes are responsible for this sensitivity.

For a given base flow U, the procedure for computing the sensitivity of an eigenvalue σ to base-flow modifications may be summarized as follows:

(*a*) solve the direct generalized eigenvalue problem (2.3) to select the eigenvalue σ and the global mode $(\hat{\boldsymbol{u}}, \hat{p})$,

(*b*) solve the adjoint stability problem (2.7) to obtain the adjoint global mode $(\hat{\boldsymbol{u}}^+, \hat{p}^+)$,

(*c*) normalize the adjoint global mode using (2.8),

(*d*) compute the sensitivity to base-flow modifications $\nabla_U \sigma$ with (2.6).

2.2. *Sensitivity to a steady force*

In this subsection the given eigenvalue σ is viewed as a function of the steady force $\boldsymbol{F}$ instead of a function of the base flow $\boldsymbol{U}$. To derive the analysis of sensitivity to a steady force, we consider small variations $\boldsymbol{\delta F}$ of the body force $\boldsymbol{F}$, which induce variations $\boldsymbol{\delta U}$ of the base flow through equations (2.2), but which do not need to be explicitly considered in the present analysis. Similarly to the analysis of §2.1, variations of a particular eigenvalue $\delta\sigma$ due to small variations $\boldsymbol{\delta F}$ of the body force are determined by

$$\delta\sigma = (\nabla_F \sigma, \boldsymbol{\delta F}), \qquad (2.9)$$

where $\nabla_F \sigma$ now defines the so-called sensitivity to a modification of the steady force, which we hereinafter term sensitivity to a steady force for conciseness. As above, $\nabla_F \sigma$ is a complex vector field, and the growth rate and frequency sensitivities may also be respectively defined as $\nabla_F \lambda = \text{Re}\{\nabla_F \sigma\}$ and $\nabla_F \omega = -\text{Im}\{\nabla_F \sigma\}$.

The derivation of $\nabla_F \sigma$ again involves a Lagrangian-based approach (detailed in Appendix A) which yields the following expression:

$$\nabla_F \sigma = \boldsymbol{U}^+, \qquad (2.10)$$

where $(\boldsymbol{U}^+, P^+)$ are the adjoint (complex) variables of the base flow. They satisfy the adjoint base-flow equations, which consist of a non-homogeneous, non-degenerate, linear problem:

$$-\nabla \boldsymbol{U}^+ \cdot \boldsymbol{U} + (\nabla \boldsymbol{U})^T \cdot \boldsymbol{U}^+ - \nabla P^+ - Re^{-1} \nabla^2 \boldsymbol{U}^+ = \nabla_U \sigma, \quad \nabla \cdot \boldsymbol{U}^+ = 0, \qquad (2.11)$$

with $\boldsymbol{U}^+ = \boldsymbol{0}$ at the inlet and on the solid walls and symmetrical boundary conditions on the lateral boundaries. The boundary conditions at the outlet are given in Appendix A. These equations are seen to involve the sensitivity to base-flow modifications $\nabla_U \sigma$, determined by equation (2.6). Note that the adjoint base-flow velocity $\boldsymbol{U}^+$ and thus the sensitivity $\nabla_F \sigma$ are divergence-free fields, unlike $\nabla_U \sigma$. It is also worth noting that the adjoint base-flow equations (2.11) are formally close to the adjoint perturbation equations (2.7). Indeed, we again observe a term related to the upstream transport of the perturbations by the base flow $-\nabla(\,)\cdot\boldsymbol{U}$ and an adjoint production term $(\nabla \boldsymbol{U})^T \cdot (\,)$. However a major difference is that equation (2.11) involves no frequency term $\sigma^*(\,)$, making the linear problem non-degenerate. Also, the presence of a complex source term equal to $\nabla_U \sigma$ makes it non-homogeneous.

The procedure to compute the sensitivity of an eigenvalue σ to a steady force may be summarized as follows:

(*a*) solve the steady Navier–Stokes equations (2.2),

(*b*) compute the sensitivity to base-flow modifications $\nabla_U \sigma$ with (2.6) as shown in §2.1,

(*c*) solve the adjoint base-flow equations (2.11) to obtain the adjoint base flow $(\boldsymbol{U}^+, P^+)$, that yields the sensitivity $\nabla_F \sigma$ through (2.10).

2.3. *Link between the two sensitivity analyses*

We now provide a link between the sensitivity analysis to a steady force developed in §2.2 and the sensitivity to base-flow modifications presented in §2.1. We have already noted in §2.2 that the source term in the adjoint base-flow equations (2.11) expresses the sensitivity to base-flow modifications $\nabla_U \sigma$. It is thus a prerequisite to the determination of the sensitivity to a steady force. In fact, the role of these adjoint base-flow equations may be viewed as to particularize the sensitivity analysis from arbitrary base-flow modifications $\boldsymbol{\delta U}$ to the specific base-flow modifications induced

by a steady force $\delta\boldsymbol{F}$. For clarity these specific base-flow modifications are hereinafter denoted $\delta\boldsymbol{U}_F$.

When a steady force is considered in equations (2.2), the base flow is a function of this force, i.e. $\boldsymbol{U}(\boldsymbol{F})$. As a consequence, a small-amplitude modification of the steady force $\delta\boldsymbol{F}$ in the flow induces the specific base-flow modification expressed as $\delta\boldsymbol{U}_F = \nabla_F\boldsymbol{U}\cdot\delta\boldsymbol{F}$, where the linear operator $\nabla_F\boldsymbol{U}$ solves the following non-homogeneous non-degenerate linear problem:

$$\nabla\delta\boldsymbol{U}_F\cdot\boldsymbol{U} + \nabla\boldsymbol{U}\cdot\delta\boldsymbol{U}_F + \nabla\delta P - Re^{-1}\nabla^2\delta\boldsymbol{U}_F = \delta\boldsymbol{F}, \quad \nabla\cdot\delta\boldsymbol{U}_F = 0, \qquad (2.12)$$

with the same boundary conditions as for the perturbation equations. Variations of the eigenvalue $\delta\sigma$ due to a small-amplitude modification of the steady force $\delta\boldsymbol{F}$ have been shown in §2.2 to be directly related to this force by (2.9). They may also be determined by applying the analysis of sensitivity to base-flow modifications not to arbitrary base-flow modifications $\delta\boldsymbol{U}$ but instead to the specific base-flow modifications $\delta\boldsymbol{U}_F$, solutions of (2.12), which are

$$\delta\sigma = (\nabla_U\sigma, \delta\boldsymbol{U}_F)$$
$$= (\nabla_U\sigma, \nabla_F\boldsymbol{U}\cdot\delta\boldsymbol{F}). \qquad (2.13)$$

Note that a comparison of (2.9) and (2.13) shows that the linear operator involved in the adjoint base-flow equations (2.11) corresponds to the inverse of the adjoint operator of $\nabla_F\boldsymbol{U}$. The interest of the analysis of sensitivity to a steady force developed in §2.2 compared to the present analysis is that variations $\delta\sigma$ due to $\delta\boldsymbol{F}$ may be directly determined from knowledge of the sensitivity function $\nabla_F\sigma$ without having to compute the specific base-flow modifications $\delta\boldsymbol{U}_F$.

3. Flow configuration and numerical approach

The general formalism developed in the previous section is applied to a specific flow configuration that is now detailed. We consider a cylinder of diameter D in a uniform upstream flow of velocity U_∞. The flow quantities are governed by the Navier–Stokes equations (2.1) made non-dimensional with these reference length and velocity scales, the Reynolds number being then defined as $Re = U_\infty D/\nu$. The geometry is defined in a Cartesian coordinate system (x, y), whose origin is located at the centre of the cylinder, and is shown in figure 1. It is delimited by the cylinder wall Γ_w and by the external boundaries, Γ_i (inlet), Γ_o (outlet), Γ_u and Γ_l (upper and lower boundaries), which are respectively located at $\sqrt{x^2 + y^2} = 0.5$, $x = x_{-\infty}$, $x = x_{+\infty}$, $y = y_{+\infty}$ and $y = y_{-\infty}$. A no-slip boundary condition $\boldsymbol{u} = \boldsymbol{0}$ is applied on Γ_w and the following boundary conditions are applied on the external boundaries: Dirichlet boundary conditions $(u, v) = (1, 0)$ on Γ_i, outflow boundary conditions $p\,\boldsymbol{n} - Re^{-1}\nabla\boldsymbol{u}\cdot\boldsymbol{n} = \boldsymbol{0}$ on Γ_o, and symmetric boundary conditions $(\partial_y u = 0, v = 0)$ on Γ_u and Γ_l.

The numerical approach is based on a finite element method. All the equations which are solved in the paper are first rewritten in a variational formulation and then spatially discretized using a mesh composed of triangular elements. The FreeFem++ software (http://www.freefem.org) is used to generate the triangulation with the Delaunay–Voronoi algorithm. The mesh refinement is controlled by the number of vertices on the external and internal boundaries. These internal boundaries are depicted in figure 1 by the dashed and dash-dotted lines and have been introduced only to control the mesh refinement. In particular, no boundary conditions are applied on these internal boundaries. The unknown velocity and pressure fields (u, v, p) are spatially discretized using a basis of Taylor–Hood (P_2, P_2, P_1) elements. All the discrete
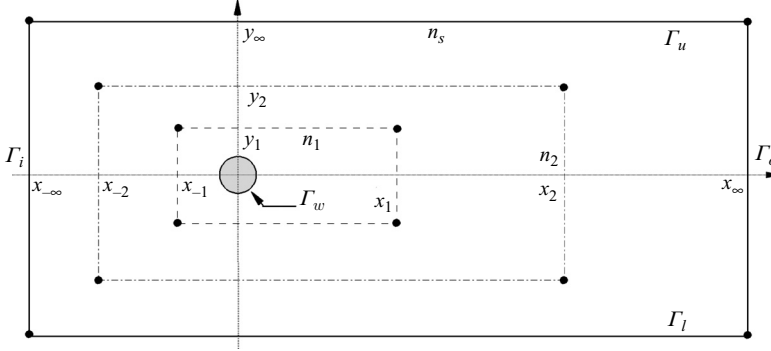
FIGURE 1. Mesh structure for the cylinder flow. The cylinder is placed in a rectangular box (solid line) delimited by the inlet, outlet, upper and lower boundaries. $x_{-\infty} = -110$, $x_{\infty} = 170$, $y_{\infty} = 90$ and $-y_{\infty}$ stand for their respective locations. The vertex densities on these boundaries are equal to $n_s = 2$. Two internal rectangular boxes (dashed and dash-dotted lines), denoted by subscript 1 and 2, are defined to control the refinement of the mesh. Their location is given by $x_{-1/-2} = -5/-40$, $x_{1/2} = 15/100$ and $y_{1/2} = 2.5/25$. The vertex densities on the boundaries of these inner boxes are given by $n_{1/2} = 50/25$. The vertex density on the cylinder wall is $n_w = 100$. The total number of triangles n_t and vertices n_v are respectively $n_t \sim 375000$ and $n_v \sim 188\,000$.

matrices resulting from the projection of the variational formulations onto the basis of finite elements are constructed with the FreeFem++ software. These matrices are sparse and their inverses are handled using the UMFPACK library, which consists of a sparse direct LU solver (see Davis & Duff 1997; Davis 2004).

The nonlinear base-flow equations (2.2) are solved via a Newton–Raphson iterative method. At each step, a matrix inversion is performed by use of the UMFPACK library. The spatial discretization of the direct (2.3) and adjoint (2.7) stability problems results in large-scale generalized eigenvalue problems. They are solved by use of the ARPACK library (http://www.caam.rice.edu/software/ARPACK) which is based upon an algorithmic variant of the Arnoldi process called the Implicitly Restarted Arnoldi Method (see Sorensen 1992). The use of a shift- and-invert strategy enables eigenvalues to be obtained in the vicinity of a given complex shift. In particular, the use of a purely imaginary shift enables the eigenvalues of largest real part to be obtained, which are of interest in hydrodynamical stability problems. Finally the linear adjoint base-flow equations (2.11) are solved by performing a matrix inversion.

4. Global stability and sensitivity results

We shall now apply the global stability and sensitivity analyses presented in §2 to the cylinder flow configuration described in §3. From now, the cylinder flow referred to is the unforced cylinder flow which is a solution of the Navier–Stokes equations (2.1) with $f = 0$. Similarly, the base flow referred to is the unforced base flow which is solution of the steady Navier–Stokes equations (2.2) with $F = 0$.

The cylinder flow is known to become unstable at a critical Reynolds number $Re_c \approx 47$. In §4.1, the stability of the base flow is investigated in the framework of global stability theory. Results are compared to data available in the literature. Sensitivity analyses are then performed at the critical Reynolds number Re_c for the leading global mode σ. In §4.2, results of the sensitivity analysis to base-flow modifications are described and interpreted to determine where physical mechanisms giving rise to the global instability are active. In §4.3, the sensitivity analysis to a
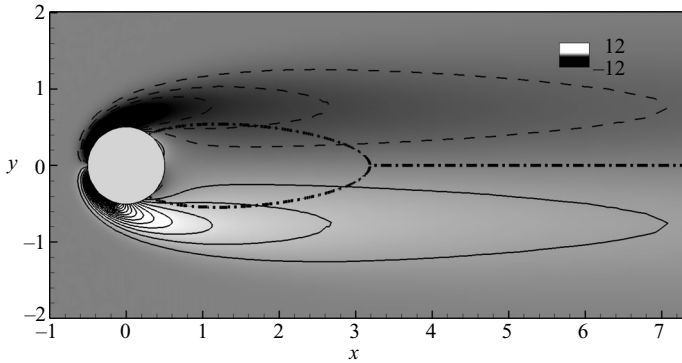
FIGURE 2. Cylinder base flow: spatial distribution of the vorticity for the critical Reynolds number $Re = 46.8$. The dash-dotted line is the dividing streamline delimiting the recirculation flow. Only a small portion of the computational domain is shown.
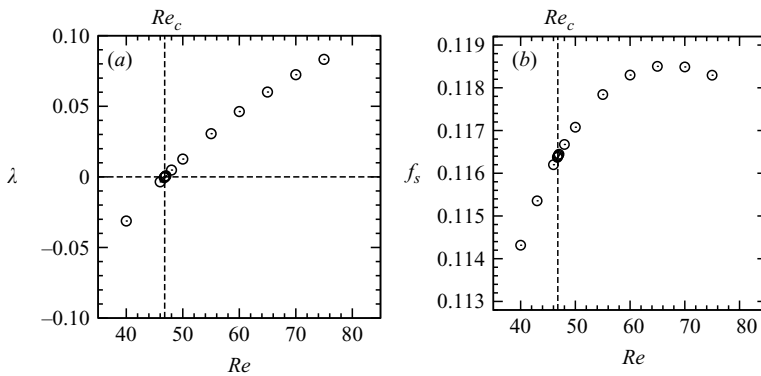

FIGURE 3. Cylinder flow. (*a*) Growth rate λ and (*b*) frequency $f_s = \omega/2\pi$ of the leading global mode as a function of the Reynolds number Re. The critical Reynolds number Re_c is shown by the vertical dashed line.

steady force is performed to predict the placement and optimize the orientation of a local steady force that aims to stabilize the flow.

4.1. *Cylinder base flow and global modes*

The steady base flow computed with the technique described above is depicted in figure 2 for $Re = 46.8$. The spatial distribution of the vorticity $\Omega = \partial_x V - \partial_y U$ is antisymmetric with respect to the centreline $y = 0$. Largest values of the vorticity are found on the upstream cylinder surface. Downstream, two shear layers displaying vorticity of opposite sign detach from the cylinder surface, delimiting a symmetric recirculation bubble (dash-dotted line in all the figures of this paper). The length of this recirculation region, measured from the rear stagnation point, is $L = 3.2$ and compares well with the literature.

The global stability of the base flow is investigated by looking for the leading global mode $(\hat{\boldsymbol{u}}, \hat{p})$, defined as the global mode of largest growth rate. The growth rate λ and frequency $f_s = \omega/2\pi$ of the leading global mode are plotted as a function of the Reynolds number, respectively in figures 3(*a*) and 3(*b*). The growth rate crosses the real axis at the critical Reynolds number $Re_c = 46.8 \pm 0.05$ when the base flow becomes unstable. This value of the critical Reynolds number is in good agreement with
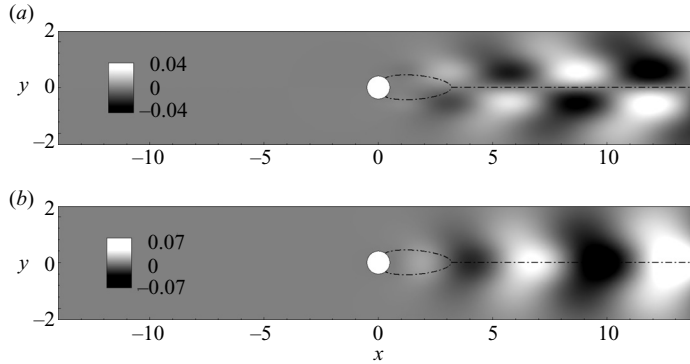
FIGURE 4. Leading global mode at the bifurcation $Re_c = 46.8$. Real part of (a) the streamwise velocity $\text{Re}(\hat{u})$ and (b) the cross-stream velocity $\text{Re}(\hat{v})$. The dash-dotted line is the dividing streamline. Only a small portion of the computational domain is shown.
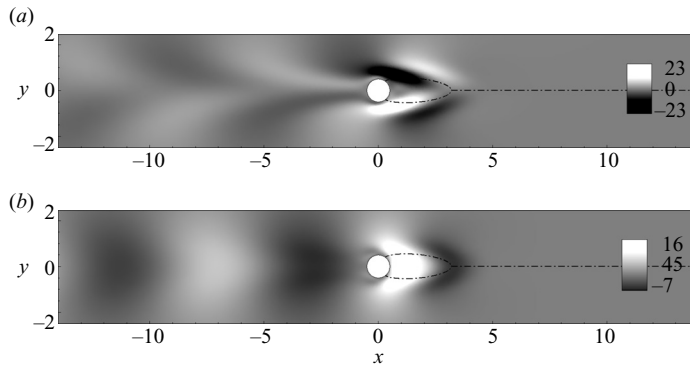

FIGURE 5. Leading adjoint global mode at the bifurcation $Re_c = 46.8$. Real part of (a) the streamwise velocity $\text{Re}(\hat{u}^+)$ and (b) the cross-stream velocity $\text{Re}(\hat{v}^+)$. The dash-dotted line is the dividing streamline. Only a small portion of the computational domain is shown.

global stability results of Jackson (1987), Barkley (2006) ($Re_c \sim 46$) and Giannetti & Luchini (2007) ($Re_c \sim 46.7$) and with the threshold of 47 observed in experiments (see Mathis, Provansal & Boyer 1984; Provansal *et al.* 1987; Williamson 1996). The small discrepancies between the present and existing results are probably due to different blockage effects. At this Reynolds number, the frequency given by the global stability analysis is equal to $f_{s,c} = \omega_c/(2\pi) \sim 0.116$, which is in good agreement with the results of Giannetti & Luchini (2007) ($f_{s,c} \sim 0.118$). Note that the global stability analysis of the base flow fails to capture the frequency of the vortex shedding for Reynolds numbers above Re_c (for further details, see Barkley 2006; Sipp & Lebedev 2007).

The leading global mode is depicted in figure 4 by the real part of its velocity field. The mode is antisymmetric and propagates downstream, since the real and imaginary parts of the velocity field are nearly in spatial quadrature (not shown here). The y-averaged energy of the perturbation grows spatially downstream and reaches a maximal value far downstream from the cylinder, at the station $x \approx 25$. The adjoint of the leading global mode ($\hat{u}^+, \hat{p}^+$) is shown in figure 5, with the same convention as for the direct mode. The streamwise (figure 5a) and cross-stream (figure 5b) velocities have the same symmetry as the direct global mode. They exhibit spatial oscillations
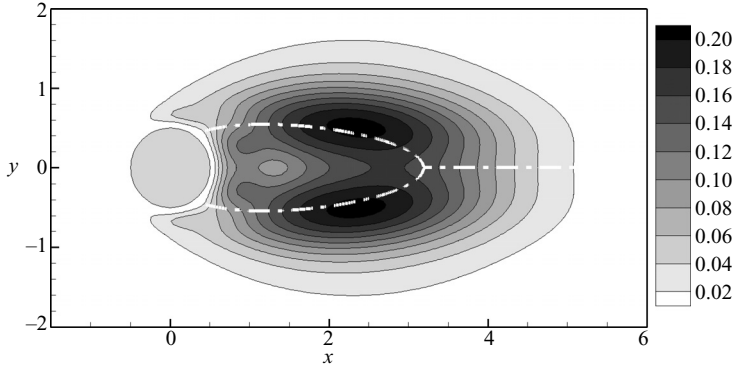
FIGURE 6. Sensitivity to a local feedback of the bifurcating global mode. The overlapping region, defined as the product of the direct and adjoint velocity magnitudes $||\hat{\boldsymbol{u}}|| \cdot ||\hat{\boldsymbol{u}}^+||$, is shown for the critical Reynolds number $Re_c = 46.8$.

but upstream from the cylinder. The maximum value of the adjoint velocity magnitude is reached close to the cylinder, at the station ($x = 0.34$, $y = 0.59$). The downstream and upstream localization of the direct and adjoint global modes result from the non-normality of the linearized Navier–Stokes equations arising from the opposite, i.e. downstream and upstream, transport of the perturbations by the base flow in the direct and adjoint linear operators (see Chomaz 2005).

Giannetti & Luchini (2007) have introduced the concept of a wavemaker in the global framework by identifying regions of the flow where generic structural modifications of the stability problem produce the strongest drift of the leading eigenvalue. To determine this wavemaker region in the flow, they have studied variations of the leading eigenvalue due to the existence of a spatially localized feedback in the momentum equations. The structural modification of the stability problem consists of introducing into equations (2.3) a force $\hat{\boldsymbol{f}}(x, y)$ proportional to the global mode velocity $\hat{\boldsymbol{u}}$. If the feedback process is assumed to be localized at the station (x_0, y_0), it is then mathematically described by

$$\hat{\boldsymbol{f}} = \boldsymbol{C}_0 \delta(x - x_0, y - y_0) \hat{\boldsymbol{u}}, \qquad (4.1)$$

where $\boldsymbol{C}_0$ is a matrix operator and $\delta(x - x_0, y - y_0)$ is the Kronecker symbol. Giannetti & Luchini (2007) have shown that

$$|\delta\sigma(x_0, y_0)| \leqslant ||\boldsymbol{C}_0|| \cdot ||\hat{\boldsymbol{u}}(x_0, y_0)|| \cdot ||\hat{\boldsymbol{u}}^+(x_0, y_0)|| \qquad (4.2)$$

if the adjoint global mode is normalized with (2.8). They then argued that the leading eigenvalue is sensitive to a local feedback only in the overlapping region of the direct and adjoint global modes. In figure 6 the product of the magnitude of the direct and adjoint velocities $||\hat{\boldsymbol{u}}|| \cdot ||\hat{\boldsymbol{u}}^+||$ is plotted. This figure recovers precisely the results of Giannetti & Luchini (2007) and thus validates the present computations. The approach of the present paper follows their line of thought, but puts more emphasis on the role of the base flow in the perturbation dynamics.

4.2. *Sensitivity to base-flow modifications*

We now consider structural modifications of the stability problem arising from base-flow modifications and compute the sensitivity to base-flow modifications $\nabla_U \sigma$ defined in equation (2.6) for the critical Reynolds number Re_c. The growth rate sensitivity $\nabla_U \lambda$ is plotted in figure 7(a) and the frequency sensitivity $\nabla_U \omega$ in figure 7(b). The
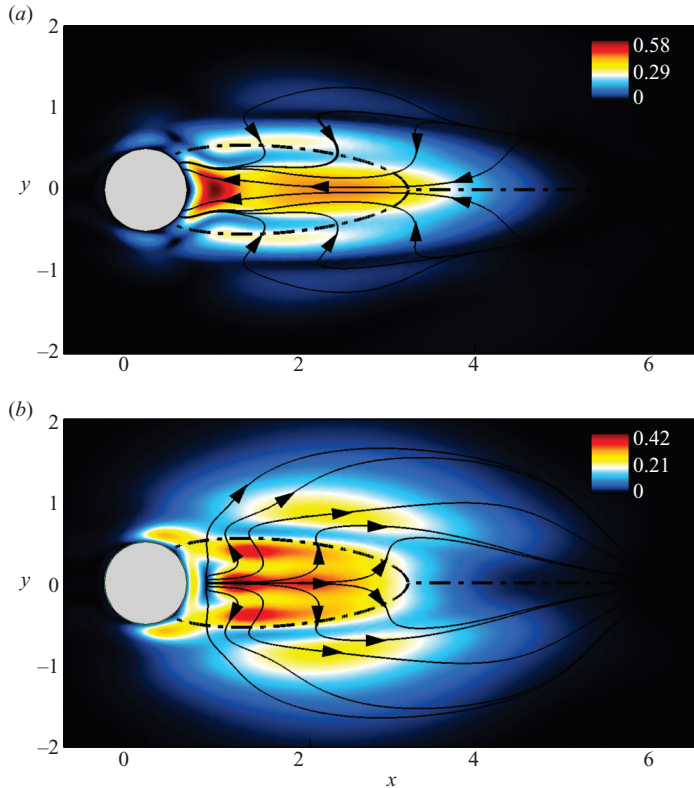
FIGURE 7. Sensitivity to base-flow modifications $\nabla_U \sigma$ of the leading eigenvalue σ for the critical Reynolds number $Re_c = 46.8$. Spatial distribution of (*a*) the growth rate sensitivity $\nabla_U \lambda$ and (*b*) the frequency sensitivity $\nabla_U \omega$. The magnitude of the growth rate and frequency sensitivities is visualized by colours and their orientation by arrows.

sensitivities $\nabla_U \lambda$ and $\nabla_U \omega$ are two-dimensional real vector fields represented both by streamlines, giving the local orientation of the sensitivity fields, and by colours indicating their magnitude. Far from the cylinder the sensitivities decay to zero due to the spatial separation of the direct and adjoint global modes. Highest magnitudes are reached inside the recirculation region, close to the rear stagnation point for the growth rate sensitivity, and further downstream for the frequency sensitivity. Now, let us consider an arbitrary base-flow modification δU that, anywhere in the flow, is oriented in the same direction as the growth rate sensitivity (see figure 7*a*). The variation of the growth rate is then positive ($\delta \lambda > 0$) which indicates a destabilization of the flow. According to figure 7(*a*), an increase of the backflow velocity in the recirculation bubble, for instance, thus has a destabilizing effect. The effect of such an increase of the backflow velocity on the frequency variation is then given by examining the frequency sensitivity. According to figure 7(*b*) it results in a decrease of the frequency since δU is oriented in the opposite direction to the frequency sensitivity.

We note that the sensitivity to base-flow modifications developed in the present paper (see figure 7) identifies regions of the flow different from the wavemaker region introduced by Giannetti & Luchini (2007) (see figure 6): the downstream part of the recirculation bubble for the former, and the upstream part of the recirculation
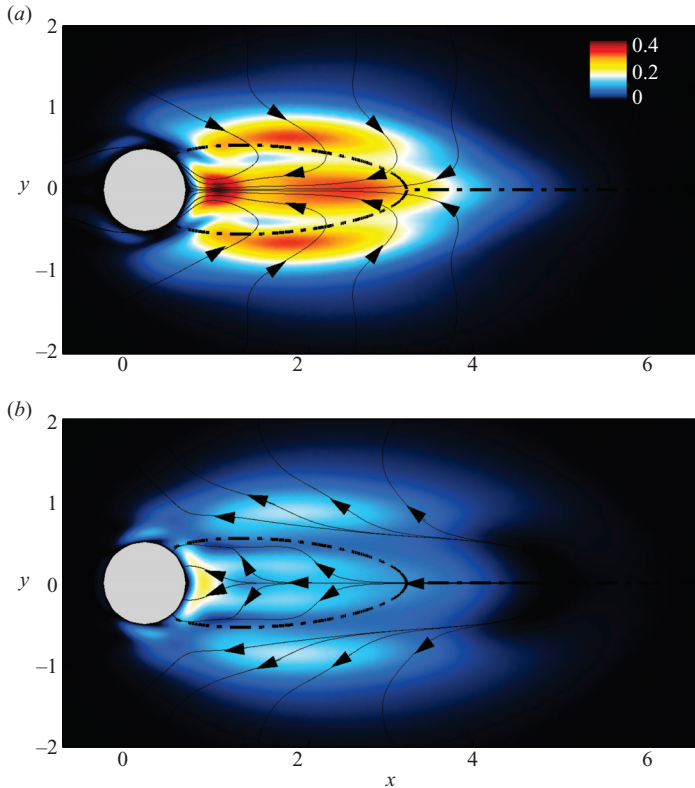
FIGURE 8. Sensitivity to base-flow modifications of the growth rate $\nabla_U \lambda$ for the critical Reynolds number $Re_c = 46.8$. This sensitivity function is decomposed into (a) a sensitivity function to modifications of the production $\nabla_{U,P} \lambda$ and (b) a sensitivity function to modifications of the transport $\nabla_{U,T} \lambda$. The magnitude of the sensitivity functions is visualized by colours and their orientation by arrows.

bubble for the latter. The link between the present analysis and the identification of the wavemaker region remains to be specified.

The global behaviour of a flow is generally viewed as the result of a competition between mechanisms of production and mechanisms of transport of perturbations by the base flow (see Huerre & Monkewitz 1990). In the local stability theory, this competition has been formalized via the concept of convective and absolute instabilities. Locally, if the production of a perturbation dominates its transport by the base flow, the flow is said locally absolutely unstable. The existence of a global instability is then conditioned to the presence of an absolutely unstable region with a finite spatial extent (see Chomaz, Huerre & Redekopp 1988). It turns out that this distinction between production and transport of perturbations appears naturally in the present sensitivity analysis. Indeed, as seen in equation (2.6), the sensitivity to base-flow modifications $\nabla_U \sigma$ is composed of a term measuring the sensitivity to modifications of the transport $\nabla_{U,T} \sigma$ and a term measuring the sensitivity to modifications of the production $\nabla_{U,P} \sigma$. Figure 8 shows this decomposition for the leading eigenvalue σ. The sensitivity to modifications of production $\nabla_{U,P} \sigma$ (resp. transport $\nabla_{U,T} \sigma$) is depicted in figure 8(a) (resp. figure 8b). The spatial distribution of their respective magnitudes is similar, but highest values are observed for the

sensitivity to modifications of production. This indicates that the sensitivity of the eigenvalue is predominantly linked to modifications of the production mechanisms. Of particular interest is to compare the relative orientation of the sensitivity fields in the two figures. In the recirculation region, both sensitivity fields have the same orientation, whereas in the outer region, they are opposite to each other. For instance, let us consider an increase of the base-flow velocity in the outer region. It corresponds to a base-flow modification δU oriented downstream. Such a base-flow modification is then oriented in the same direction as the sensitivity to production (see figure 8a), and therefore contributes to a destabilization via the production mechanism ($\delta\lambda > 0$). Now, according to figure 8(b), the same δU is oriented in the opposite direction to the sensitivity to transport and therefore contributes to a stabilization via the transport mechanism ($\delta\lambda < 0$). As a consequence, in the outer region where the relative orientation of the sensitivity functions is opposite, the mechanisms of production and transport are opposing. And inversely, in the recirculation region where the sensitivity functions have same orientation, the mechanisms of production and transport cooperate.

The sensitivity analysis to base-flow modifications is appropriate to theoretically determine regions and properties of the base flow that play a role in the onset of vortex shedding behind the cylinder. To know where and how the base flow should be modified to stabilize the leading global mode is a first step in controlling the flow. However, arbitrary base-flow modifications are not physically relevant and this analysis does not answer the question of how to produce 'physical' base-flow modifications that would stabilize the flow.

4.3. *Sensitivity to a steady force*

We are now interested in the stabilization of cylinder flow by use of a steady force that is assumed to only modify the base flow. To that end, the sensitivity analysis to a steady force, presented in §2.2, is applied to the leading eigenvalue σ. Note that, since the cylinder base flow is solution of the steady Navier–Stokes equations with $F = 0$, the steady force is denoted δF in agreement with the general formalism developed in §2. We recall that, thanks to the sensitivity analysis to a steady force, base-flow modifications induced by δF do not need to be explicitly computed in order to determine the eigenvalue variations $\delta\sigma$.

Figure 9 shows the sensitivity to a steady force $\nabla_F \sigma$ of the leading eigenvalue σ computed for the critical Reynolds number Re_c. The spatial distributions of the growth rate $\nabla_F \lambda$ and frequency $\nabla_F \omega$ sensitivities are respectively depicted in figures 9(a) and 9(b). Three regions in the vicinity of the cylinder and extending a few diameters downstream may be identified: the *separation region* that, from now on, refers to the region in the close vicinity of the separation point on the cylinder, the *recirculation region*, delimited by the dividing streamline, and the *outer region* corresponding to the region half a diameter in size surrounding the recirculation region. Two strong local maxima of the growth rate sensitivity to a steady force (see figure 9a) may be distinguished. The first is located in the separation region and the second in the recirculation region, close to the centreline. A weaker local maxima is located in the outer region. Let us consider a steady force of unit magnitude applied locally in the flow. A local force oriented in the opposite direction to the arrows plotted in figure 9(a) induces a negative variation of the growth rate ($\delta\lambda < 0$) which is proportional to the local magnitude of the sensitivity function. Therefore, in the separation and recirculation regions, a local force is stabilizing when oriented downstream. The opposite is true in the outer region. Since, as shown in figure 7(b),
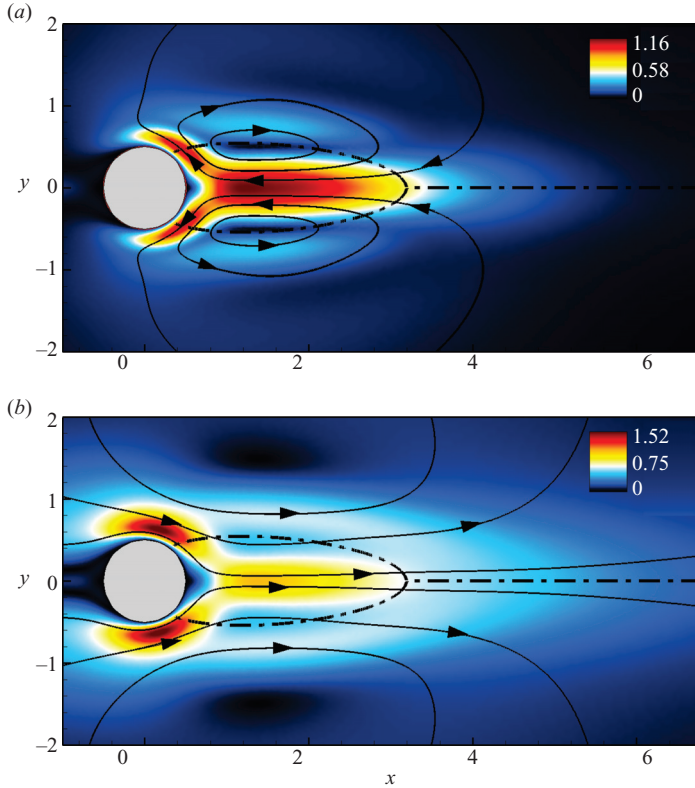
FIGURE 9. Sensitivity to a steady force $\nabla_F \sigma$ of the leading eigenvalue σ for the critical Reynolds number $Re_c = 46.8$. Spatial distribution of (a) the growth rate sensitivity $\nabla_F \lambda$ and (b) the frequency sensitivity $\nabla_F \omega$. The magnitude of the growth rate and frequency sensitivities is visualized by colours and their orientation by arrows.

the frequency sensitivity function is oriented downstream everywhere in the flow, a stabilizing local force is associated with an increase of the frequency in both the separation and recirculation regions, and with a decrease of the frequency in the outer region. Note that if a local force had been used here to interpret the sensitivity maps seen in figure 9, the present approach would also enable prediction of whether a non-local force has a stabilizing or destabilizing effect.

5. Sensitivity analysis and passive control of cylinder flow

Strykowski & Sreenivasan (1990) have experimentally investigated how a small control cylinder appropriately placed in the wake of the main cylinder could alter or even suppress vortex shedding. Supposing that the appearance of the vortex shedding was linked to a global instability they proposed an experimental estimation of its temporal growth rate through local measurements of the velocity fluctuations, denoted a_r. They showed that suppression of the vortex shedding was correlated with negative temporal growth rates. For a control cylinder whose diameter d is ten times smaller than the main cylinder, i.e. $d = 0.1$, they determined the locus of all points in the (x, y)-plane corresponding to zero temporal growth rate measurements ($a_r = 0$). Figure 10, obtained from their experimental results, depicts, for various values of the Reynolds number, the regions of finite spatial extent within which the placement of
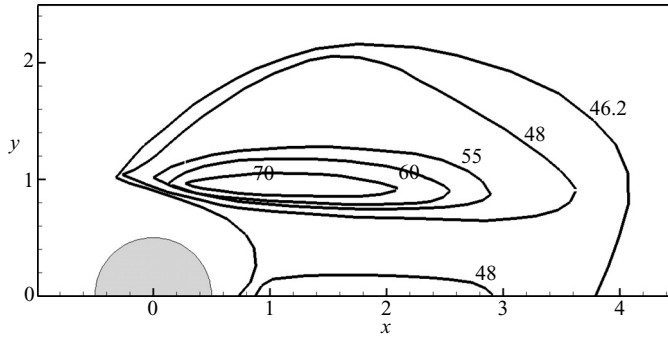
FIGURE 10. Results of passive control by Strykowski & Sreenivasan (1990). A control cylinder 10 times smaller than the main cylinder is placed at various locations of the flow. For each location of the control cylinder and for various Reynolds numbers, the growth rate a_r of the perturbations is measured. Contours where the growth rate is nil ($a_r = 0$) are represented for each Reynolds number.

the control cylinder suppresses the vortex shedding. For a Reynolds number close to the critical Reynolds number ($Re = 48$), the vortex shedding is suppressed if the control cylinder is placed either in the outer region or inside the recirculation region. When the Reynolds number is increased, the stabilizing region inside the recirculation region vanishes and the spatial extent of the stabilizing region inside the outer region is reduced. Note that the vortex shedding is never suppressed if the control cylinder is located in the separation region.

In this section, we attempt to retrieve these results using the sensitivity analysis to a steady force. We propose to model the presence of the small control cylinder by a point source of momentum f in the Navier–Stokes equations (2.1), applied at the location of the control cylinder centre (x_0, y_0). First, note that, whatever the position of the control cylinder, its wake is steady due to the low Reynolds number based on the control cylinder diameter and the local velocity of the base flow. The force exerted by the flow on the control cylinder is therefore steady and may be characterized in direction and intensity using a low-Reynolds-number model. By the action and reaction principle, the control cylinder exerts a force of the same strength but of opposite direction on the flow. The presence of this force in the momentum equations governing the base flow simulates the presence of the control cylinder. If the diameter of the control cylinder is sufficiently small, such a force may be localized at the station (x_0, y_0) where the control cylinder is placed. The effect of a control cylinder on the flow stability can now be investigated using the sensitivity analysis to a steady force.

5.1. *Sensitivity for a Reynolds number close to the bifurcation:* $|Re - Re_c| \leqslant 0.1$

The control of the unsteady wake is first investigated at the critical Reynolds number $Re_c = 46.8 \pm 0.05$. The introduction of the control cylinder at (x_0, y_0) into the flow is modelled by a steady force localized at the same station. This force is applied to the unforced base flow, solution of equations (2.2) with $F = 0$, and is therefore denoted δF according to the general formalism developed in §2.2. For simplicity, this steady force is first considered to be proportional to the square of the steady velocity, i.e.

$$\delta F(x, y) = -\alpha \, ||U|| \, U \, \delta(x - x_0, y - y_0), \tag{5.1}$$
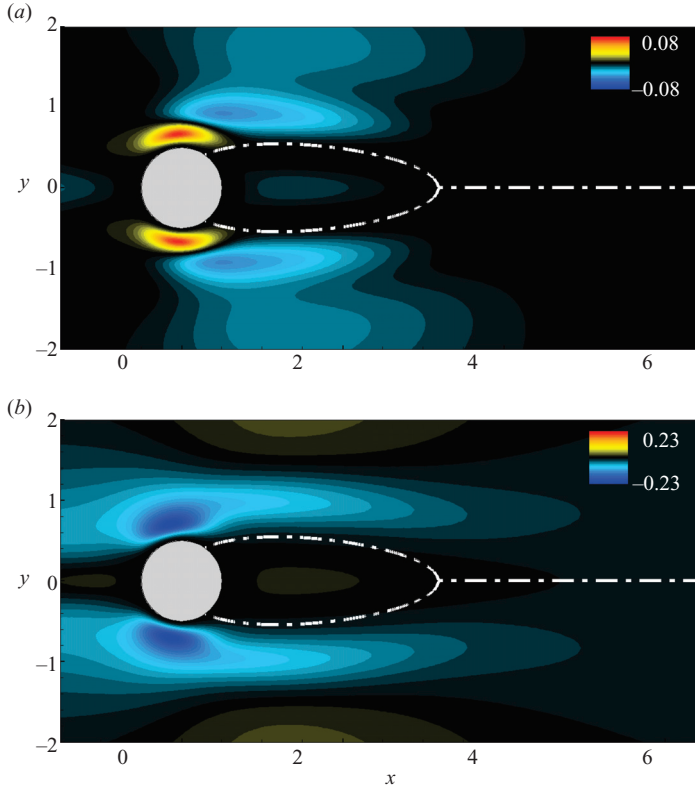
FIGURE 11. Variations of (*a*) the growth rate $\delta\lambda/\alpha = -\nabla_F\lambda(x_0, y_0)\cdot\boldsymbol{U}(x_0, y_0)$ and (*b*) the frequency $\delta\omega/\alpha = -\nabla_F\omega(x_0, y_0)\cdot\boldsymbol{U}(x_0, y_0)$ as a function of the location of the steady force modelled by equation (5.1). Results are given for the critical Reynolds number $Re = 46.8$.

where α is a positive coefficient which is assumed small in this section, $0 < \alpha \ll 1$. Effects of nonlinearities, i.e. values of α of unit order, are explored in Appendix B.

Using the force modelled in equation (5.1), variations of the growth rate and frequency may be derived from equations (2.5). We obtain

$$\delta\lambda(x_0, y_0) = -\alpha\,\|\boldsymbol{U}(x_0, y_0)\|\,\nabla_F\lambda(x_0, y_0)\cdot\boldsymbol{U}(x_0, y_0), \tag{5.2}$$

$$\delta\omega(x_0, y_0) = -\alpha\,\|\boldsymbol{U}(x_0, y_0)\|\,\nabla_F\omega(x_0, y_0)\cdot\boldsymbol{U}(x_0, y_0). \tag{5.3}$$

These variations are proportional to the amplitude parameter α and depend on the scalar product of the sensitivities to a steady force with the base-flow velocity. Since the base flow is marginally stable ($\lambda \approx 0$), $\delta\lambda < 0$ (resp. $\delta\lambda > 0$) corresponds to a stabilization (resp. destabilization). Figure 11 is a mapping of the variations of the leading eigenvalue induced by such a force divided by the amplitude parameter, i.e. $\delta\lambda(x_0, y_0)/\alpha$ and $\delta\omega(x_0, y_0)/\alpha$. To each spatial position (x_0, y_0) of the force is associated the resulting variations of the growth rate (figure 11*a*) and frequency (figure 11*b*). Figure 11(*a*) shows that forcing the base flow in the separation region has a destabilizing effect ($\delta\lambda > 0$) whereas forcing the base flow in the recirculation region or in the outer region has a stabilizing effect ($\delta\lambda < 0$). Figure 11(*b*) shows that the force tends to decrease the frequency ($\delta\omega < 0$) for almost every position of the control cylinder, the strongest effect being obtained in the separation region. A

weak increase of the frequency is observed ($\delta\omega > 0$) only if the force is located in the recirculation region.

These results are in qualitative agreement with the experimental results of Strykowski & Sreenivasan (1990) obtained for a Reynolds number close to the bifurcation. Comparing figure 11(a) with figure 10 shows that stabilizing and destabilizing regions are well reproduced for these Reynolds numbers. It is found that the outer and recirculation regions are stabilizing, in agreement with the results given by the experimental study at $Re = 46.2$. Also, the separation region is found to be destabilizing, which explains why Strykowski & Sreenivasan (1990) have not observed the suppression of the vortex shedding with a control cylinder placed in this region. In fact, the present analysis suggests that this result is not due to a lack of sensitivity (see figure 9a) but rather to the relative orientation of the force and the sensitivity function, which are both oriented upstream, so that $\delta\lambda > 0$. A stabilizing effect ($\delta\lambda < 0$) would have been obtained if the force was oriented downstream, but introducing a control cylinder into the flow at this location cannot produce such a force, since a cylinder only produces drag.

5.2. *Sensitivity for higher values of the Reynolds number: $Re > Re_c$*

In an attempt to quantitatively reproduce the experimental results for higher values of the Reynolds number $Re > Re_c$, the question of the amplitude of the force has to be addressed carefully. Since the growth rate $\lambda(Re)$ of the leading global mode of the unforced base flow increases with the Reynolds number, as seen in figure 3, the sign of the growth rate variation $\delta\lambda(Re)$ induced by a force is not enough to determine whether the flow is stabilized or not. In fact, the amplitude of the growth rate variation should at least be equal to $|\delta\lambda| > \lambda(Re)$ to conclude that the force stabilizes the flow. Since, in the sensitivity analysis, $|\delta\lambda|$ is directly proportional to the amplitude of the force, the latter should accurately be modelled to achieve valid predictions. To this end, the force exerted on the base flow by the control cylinder of diameter d, placed at the location (x_0, y_0), is now modelled as the opposite of the drag force exerted on a cylinder of same diameter embedded in an upstream uniform flow of velocity $\boldsymbol{U}(x_0, y_0)$. It is given by

$$\boldsymbol{\delta F}(x, y) = -\tfrac{1}{2}dC_D(Re_d)||\boldsymbol{U}(x_0, y_0)||\boldsymbol{U}(x_0, y_0)\delta(x - x_0, y - y_0), \qquad (5.4)$$

where the drag coefficient $C_D(Re_d)$ is a function of the local Reynolds number $Re_d = ||\boldsymbol{U}(x_0, y_0)||dRe$. Note that the above expression is dimensionally correct since the Dirac function is inversely proportional to a surface. Now we need to accurately determine the drag coefficient of a cylinder flow when the local Reynolds number is in the range $1 \leqslant Re_d \leqslant 10$, which are characteristic values of the local Reynolds numbers in the experiment of Strykowski & Sreenivasan (1990) for $d = 0.1$. To this end the drag coefficient is expressed by the analytical law

$$C_D(Re_d) = \frac{1}{Re_d(a + b\,\ln(Re_d))} \qquad (5.5)$$

where $a = 0.0987$ and $b = -0.0627$. These values have been determined by interpolation on values of the drag coefficient obtained through base-flow calculations of cylinder flows in the range of local Reynolds number mentioned above. Given expression (5.5) for the drag coefficient and the dependence of Re_d on the base-flow velocity, the drag force (5.4) is not proportional to the square of the base-flow velocity, as expected for this range of Reynolds number.
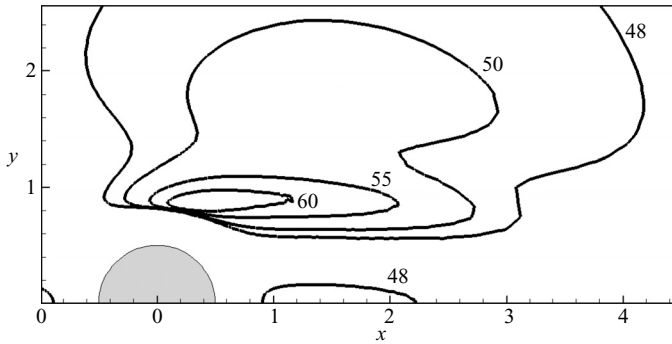
FIGURE 12. Contours where the linear estimation of the growth rate is nil, i.e. $\lambda(Re) + \delta\lambda(Re) = 0$, when the local force expressed by (5.4) is used to model the presence of the cylinder. Values of the Reynolds number are indicated in the figure. Parameter setting: $d = 0.1$

The amplitude of the modelled force given by (5.4) and (5.5) is no longer infinitesimal as in the previous subsection. The induced base-flow modifications may thus become large enough to invalidate the assumption of linearity underlying the sensitivity analysis. In this case, the base-flow modifications which are taken into account by this analysis are only a linear approximation of the base-flow modifications induced by the force (see equation (2.12)). The growth rate variation determined by means of this analysis is therefore a linear estimation of the true nonlinear growth rate variation. The latter is computed in Appendix B where the question of how the nonlinearities alter the results of the sensitivity analysis is addressed. Fortunately, it turns out that the effect of the nonlinearities does not invalidate the present linear approach.

Regions of the flow where the force modelled by equation (5.4) suppresses the instability are determined as follows. The unforced base flow $U(Re)$ and the growth rate $\lambda(Re)$ of the leading global mode are successively computed for various Reynolds numbers. The growth rate sensitivity analysis to a steady force is then carried out as described in §2.2 for each value of the Reynolds number Re: we determine the sensitivity of the growth rate $\nabla_F \lambda$ and the associated variation of the growth rate $\delta\lambda(Re) = (\nabla_F \lambda, \delta F)$ with δF given by (5.4). The growth rate variation $\delta\lambda(Re)$ term is then added to the unforced growth rate $\lambda(Re)$ to finally obtain a linear estimation of the controlled growth rate $\lambda(Re) + \delta\lambda(Re)$. Figure 12 reports for several Reynolds numbers the loci of all points in the (x, y)-plane corresponding to $\lambda(Re) + \delta\lambda(Re) = 0$. It should be compared with the experimental results of Strykowski & Sreenivasan (1990) given in figure 10. The patterns in these two figures are very similar, indicating that the sensitivity analysis predicts well the regions of the flow where the placement of a control cylinder suppresses the instability. All the features described at the beginning of this section are retrieved. For $Re = 48$, the existence of the two stabilizing regions, observed in figure 10, is reproduced well. When the Reynolds number is increased, the spatial extent of the stabilizing region in the outer region is seen to be reduced, in accordance with the experimental observations. Also the stabilizing region in the recirculation region vanishes and the spatial extent of the stabilizing outer region tends to shrink towards a region close to the cylinder. However, we note some differences with the experimental results. First, the curves obtained for Reynolds numbers $Re = 48$ and 50, exhibit concavities quite different, in the outer region, from the experimental curves, leading to predictions of a larger stabilizing region. Secondly,

for Reynolds numbers, $Re = 55$ and 60, the stabilizing region is smaller than in the experiment, and for larger Reynolds numbers it vanishes. As shown in Appendix B, the linear estimation of the growth rate variation underestimates the true nonlinear growth rate variation, which may explain why the predicted stabilizing regions are smaller for large Reynolds numbers. But this argument cannot explain why the predicted stabilizing regions are larger for Reynolds numbers close to Re_c. In fact, introducing a control cylinder in the flow modifies not only the base-flow equations but also the perturbation equations, since the velocity of the perturbations vanishes on the wall of the control cylinder. We believe that this effect, which has not been assessed by the present analysis, might explain why the extent of the stabilizing region is overestimated.

6. Physical interpretation of the stabilization for a Reynolds number close to the bifurcation: $Re = Re_c$

Strykowski & Sreenivasan (1990) have argued that the control cylinder has a stabilizing effect because it weakens the shear layer behind it by spreading out the velocity gradient over a larger distance. As a consequence the optimal placement of the control cylinder to suppress the vortex shedding should be close to the locus of maximum vorticity of the flow without control, because the reduction of the velocity shear would then be maximum. This physical interpretation is now discussed in some detail in the light of the sensitivity analysis presented in this paper. This approach has enabled us to predict the optimal placement of a small control device using the sensitivity to a steady force. Base-flow modifications induced by the force were not explicitly computed. To give a physical interpretation of the stabilizing effect of the control cylinder, it is proposed to compute these specific base-flow modifications and to analyse their effect on the stability problem using the sensitivity to base-flow modifications, as described in § 2.3.

6.1. *Analysis of the base-flow modifications induced by the local steady force*

We choose to analyse the case presented in § 5.1 where a drag force given by (5.1) and applied at the station $(x_0, y_0) = (1.2, 1)$ has a stabilizing effect on the flow. We recall that $Re = 46.8$ and that the position of the force corresponds to the station where the largest stabilization of the flow is obtained (see figure 11a). The specific base-flow modifications δU_F induced by the force δF are given by $\delta U_F = \nabla_F U \cdot \delta F$ and may be determined by solving the base-flow equations linearized around the unforced base flow (2.12). Note that the local force δF given in equation (5.1) is numerically approximated by a Gaussian function centred at (x_0, y_0). Also, to simplify the notation, we set $\alpha = 1$, keeping in mind that the force δF is of small amplitude. The computed base-flow modifications are depicted in figure 13. The two-dimensional spatial distribution of the streamwise velocity δU_F is plotted in figure 13(a). The largest magnitudes of this velocity occur in the vicinity of the station where the force is applied. However, we observe that velocity modifications remain significant far from this application point, thus confirming that a local force has a non-local effect on the base flow. The force induces a strong decrease of the velocity downstream from its application point, and a slight increase of the velocity in the rear part of the recirculation region. These base-flow modifications are more clearly seen in figures 13(b) and 13(c) that respectively depict velocity and vorticity profiles on the cross-streamline $x = 2$. In these figures, the solid and dashed lines respectively refer to the base flow and to its modifications. We observe that the velocity decreases in the
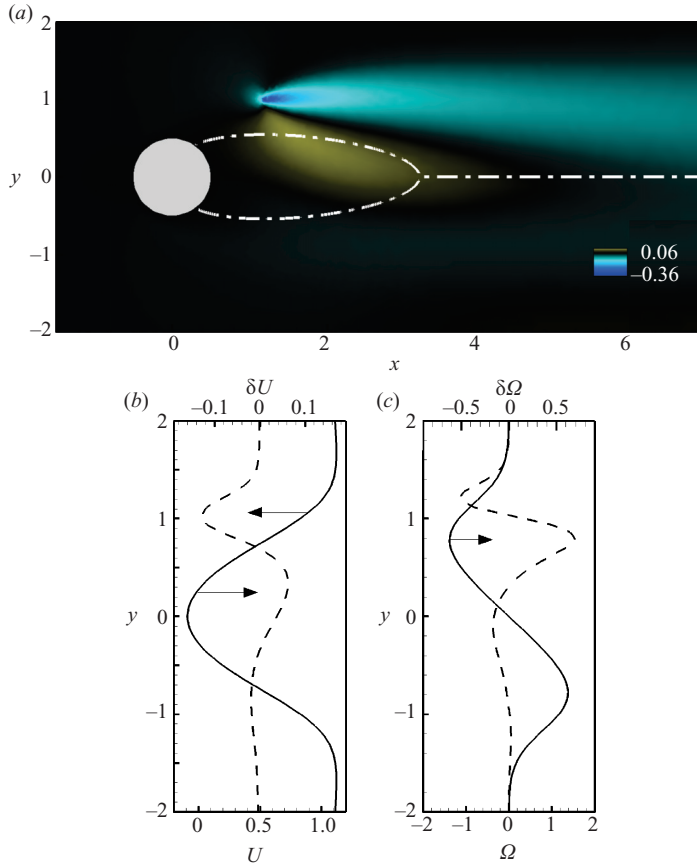
FIGURE 13. Specific base-flow modifications induced by a force modelled by equation (5.1) with $\alpha = 1$ and located at the station ($x_0 = 1.2$, $y_0 = 1.0$). The Reynolds number is close to the bifurcation: $Re = 46.8$. (a) Spatial distribution of the streamwise velocity δU_F. (b) Velocity and (c) vorticity profiles along the cross-streamline $x = 2$. The base flow is depicted by the solid lines and its modifications by the dashed lines.

high-speed part of the upper shear layer and increases in the low-speed part, as shown by the arrows in figure 13(b). This tends to reduce the magnitude of the velocity shear in the upper shear layer, the largest reduction occurring where the shear magnitude is maximal in the base flow (see arrows in figure 13c).

As outlined in §2.3, the growth rate variation induced by such a force may now be assessed by applying either the sensitivity analysis to a steady force (see equation (2.9)) or the sensitivity to base-flow modifications (see equation (2.13)). The former case is denoted $\delta\lambda_F$, the latter $\delta\lambda_U$. Results are reported in table 1 and show that the relative difference between these growth rate variations is less than 1%. The equivalence of the two sensitivity analyses is thus validated.

6.2. *Analysis of the stabilization mechanism in terms of base-flow modifications*

In this section, we analyse the contribution to the global growth rate variation $\delta\lambda$ of the specific base-flow modifications δU_F induced by the local force δF. Recalling that $\delta\lambda$ is obtained by integration over the space $\nabla_U\lambda(x, y) \cdot \delta U_F(x, y)$ (see equation (2.5)), we analyse the integrand to identify the regions in space which are responsible for the stabilization of the global mode. Figure 14(a) depicts the spatial distribution of

$\delta\lambda_F$	$\delta\lambda_U$	$\delta\lambda_{U,T}$	$\delta\lambda_{U,P}$	$\delta\lambda_{U,Tot}$
-0.01227	-0.01233	0.00873	-0.021061	-0.01234

TABLE 1. Evaluation of the leading growth rate variation $\delta\lambda$ induced by a force modelled by equation (5.1) with $\alpha = 1$ and located at the station ($x_0 = 1.2$, $y_0 = 1.0$). The Reynolds number is close to the bifurcation: $Re = 46.8$. $\delta\lambda_F$ and $\delta\lambda_U$ have been obtained respectively with the sensitivity to a steady force and the sensitivity to base-flow modifications. $\delta\lambda_{U,T}$ and $\delta\lambda_{U,P}$ are evaluations of the contribution arising respectively from modifications of the transport and production, and $\delta\lambda_{U,Tot} = \delta\lambda_{U,T} + \delta\lambda_{U,P}$ is the sum of these two contributions.
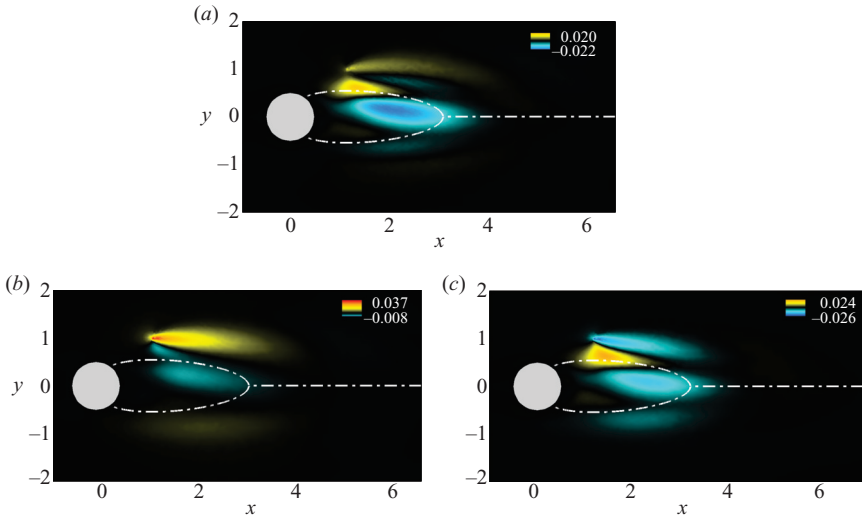

FIGURE 14. Spatial distribution of the local contributions yielding the global growth rate variation $\delta\lambda$. (a) Representation of the integrand $\nabla_U \lambda(x, y) \cdot \delta U_F(x, y)$. $\delta\lambda$ is equal to the integration over space of this quantity. This integrand may then be decomposed into a part related to (b) transport, i.e. $\nabla_{U,T} \lambda(x, y) \cdot \delta U_F(x, y)$ and a part related to (c) production of perturbations, i.e. $\nabla_{U,P} \lambda(x, y) \cdot \delta U_F(x, y)$. The force is modelled by equation (5.1) with $\alpha = 1$ and is located at the station ($x_0 = 1.2$, $y_0 = 1.0$). The Reynolds number is close to the bifurcation: $Re = 46.8$.

this integrand, i.e. $\nabla_U \lambda \cdot \delta U_F$. At a local station ($x$, y), a positive (resp. negative) value of this quantity means that the local base-flow modifications $\delta U_F(x, y)$ contribute to the destabilization (resp. stabilization) of the global mode. In the close vicinity of the application point of the force, where the strongest modifications of the base flow are observed (see figure 13), the contribution to the global growth rate variation is weak. This proves that the stabilization of the flow induced by the force is not due to base-flow modifications in the close vicinity of its application point, but rather to modifications of the base flow occurring further on. Several regions contributing either to a stabilization or to a destabilization are visible in figure 14(a). This figure indicates the complex effect of the force on the variation of the growth rate and also suggests that the stabilizing effect of the force may not be captured by performing only a local stability analysis. In fact, three large regions may be distinguished in figure 14(a): the region extending downstream of the application point of the force that weakly contributes to the destabilization of the global mode, the region below this application point which strongly contributes to its destabilization and the large blue region extending to the rear of the recirculation bubble which strongly

contributes to its stabilization. It turns out that the dominating contribution is the stabilizing contribution, thus identifying the rear of the symmetrical recirculation bubble as responsible for the stabilizing effect of this force. In fact, the weak base-flow modifications that occur in this region (see figure 13a) strongly contribute to stabilizing the global mode, because the magnitude of the sensitivity to base-flow modifications is large in this region (see figure 7a). It is striking to note that the region downstream of the application point of the force, where largest base-flow modifications occur, contributes to a destabilization. This statement is opposite to the physical interpretation proposed by Strykowski & Sreenivasan (1990).

6.3. *Analysis of the stabilization mechanism in terms of modifications of the transport and production mechanisms*

To further explore the mechanisms that stabilize the flow, the global growth rate variation is decomposed as $\delta\lambda_U = \delta\lambda_{U,T} + \delta\lambda_{U,P}$, where each term is computed by using the decomposition of the sensitivity presented in equation (2.6). $\delta\lambda_{U,T}$ measures the variation due to modifications of the transport and $\delta\lambda_{U,P}$ measures the variation due to modification of the production. Results, reported in table 1, show that $\delta\lambda_{U,P} < 0$ and $\delta\lambda_{U,T} > 0$. The overall effect of modification of the production is thus stabilizing, whereas the overall effect of modification of the transport is destabilizing. In other words, the introduction of a control cylinder severely weakens the production of perturbations ($\delta\lambda_{U,P} < 0$) while the mean downstream convection of perturbations by the base flow slows down slightly ($\delta\lambda_{U,T} > 0$). It may be claimed that modification of the production mechanisms is responsible for the stabilizing effect of the force.

The projection of the base-flow modifications onto the growth rate sensitivity to transport, i.e. $\nabla_{U,T}\lambda(x, y) \cdot \delta U_F(x, y)$, is plotted in figure 14(b). Figure 14(c) shows the growth rate sensitivity to production, i.e. $\nabla_{U,P}\lambda(x, y) \cdot \delta U_F(x, y)$. These quantities are respectively called the contributions to the growth rate variation due to the local modifications of transport and production. The similarity of the patterns seen in figures 14(a) and 14(c) is striking and indicates, again, that the local contribution is, almost everywhere, dominated by the local production effect.

Let us first focus on the rear part of the recirculation region, where it is recalled that both the backflow velocities and the velocity shear are reduced. In this region, by comparing figures 14(b) and 14(c), it is clear that both modifications of the transport and modifications of the production have a stabilizing effect. In fact, the reduction of the production of perturbations by the base flow, due to the decrease of the velocity shear, is mainly responsible for the stabilizing effect. And the increase of the downstream transport contributes only little to the stabilization.

We now examine the region downstream of the application point of the force. It is recalled that strong base-flow modifications occur in this region characterized by a decrease of both the streamwise velocity and the velocity shear. Examining figures 14(b) and 14(c) shows that modification of the transport and modification of the production have opposite effects, destabilizing for the former and stabilizing for the latter. The destabilizing effect is attributed to the reduction of the downstream transport of perturbations by the base flow, whereas the stabilizing effect is due to the reduction of the production mechanisms induced by the decrease of the velocity shear.

Finally, as proposed by Strykowski & Sreenivasan (1990), the control cylinder located at the optimal station $(x_0, y_0) = (1.2, 1)$ induces a stabilization of the flow mainly because of the reduction of the shear strength that diminishes the production mechanisms. But it is the reduction of the shear in the rear part of the recirculation region and not in the region downstream of the application point of the force which is responsible for the stabilization of the flow. In other words, the stabilization is due

to the weak increase of the velocity in the low-speed part of the shear layer, and not to the strong decrease of the velocity in the high-speed part of the shear layer.

7. Conclusion

In the present paper we have developed sensitivity analyses that aim to predict variations of the eigenvalue of global modes. When these variations result from arbitrary base-flow modifications, the sensitivity analysis is called sensitivity to base-flow modifications. When these variations result from specific base-flow modifications induced by a steady force, the sensitivity analysis is called sensitivity to a steady force. Both sensitivity analyses are based on the evaluation of gradients through adjoint methods. The sensitivity to base-flow modifications is given by introducing an adjoint stability problem and the sensitivity function is then given as the sum of two terms that depend on the direct and adjoint global modes. These two terms represent the sensitivity of the eigenvalue to modifications of the transport and production of perturbation mechanisms due to the base-flow modifications. The sensitivity to a steady force is given by introducing, in addition to the sensitivity to base-flow modifications, an adjoint base-flow problem which is forced by a source term equal to the sensitivity to base-flow modifications. These adjoint base-flow equations enable us to focus on base-flow modifications arising from a steady force. The sensitivity function is then simply the adjoint base-flow velocity.

The sensitivity analyses have then been applied to cylinder flow. For a Reynolds number close to the critical Reynolds number, the sensitivity to base-flow modifications has been used to identify the region where local base-flow modifications produce the largest eigenvalue variations. In these regions, the respective contributions of transport and production of perturbations by the base flow have been analysed, thus identifying how they contribute to the onset of global instability.

The sensitivity analysis to a steady force has enabled us to determine where and in which directions a steady force should be applied to induce the largest negative growth rate variations. A local steady force may be created locally in the flow by the introduction of a small control cylinder which exerts a force on the base flow which is opposite to its drag. A model of a local steady force is then provided to model the presence of such a control cylinder. By means of the sensitivity to a steady force, positions of the control cylinder that stabilize the flow have been predicted and compared to the experimental results of Strykowski & Sreenivasan (1990). The accuracy of the prediction validates the choice of modelling the presence of a control cylinder by a steady local force and shows that this control device suppresses the vortex shedding by inducing base-flow modifications that stabilize the leading global mode and do not destabilize the stable global modes (see Appendix C).

Finally, physical interpretation of the stabilizing effect of the force has been proposed, based on the determination of regions where base-flow modifications contribute to stabilizing the global mode. In particular it has been shown that, placed at its optimal position, the control cylinder stabilizes the flow by damping the production of perturbations in the rear of the symmetrical recirculation region. Such an approach consisting of passive control of a global instability may easily be applied to other flow configurations, for instance cavities or recirculation flows that are known to develop such global instabilities. Moreover, as the present formalism is close to the optimal control formalism, further studies might address the question of the optimization of the control cylinder diameter to suppress the vortex shedding and reduce the drag of the main cylinder.

Appendix A. Derivation of sensitivity functions

In this Appendix, we successively derive the sensitivity to a steady force and the sensitivity to base-flow modifications.

A.1. *Determination of the sensitivity to a steady force*

A.1.1. *State variables and state equations*

The state variables are the base-flow variable, now denoted by the vector $Q(x, y) = (U, P)^T = (U, V, P)^T$, and the perturbation variable, denoted by the vector $\tilde{q}(x, y, t) = (\tilde{u}, \tilde{p})^T$. The state of the base flow is governed by the steady Navier–Stokes equations (2.2) and is forced by the control variable $Q_F = (F, 0)^T$. These equations are written in a symbolic form

$$\mathbf{BF}(Q) = Q_F. \tag{A 1}$$

The boundary conditions for the base flow are

$$U = (1, 0) \quad \text{at the inlet}, \tag{A 2}$$

$$U = 0 \quad \text{on the solid walls}, \tag{A 3}$$

$$(\partial_y U, V) = (0, 0) \quad \text{on the horizontal lateral boundaries}, \tag{A 4}$$

$$P\,\boldsymbol{n} - Re^{-1}\nabla U \cdot \boldsymbol{n} = \mathbf{0} \quad \text{at the outlet}. \tag{A 5}$$

The perturbation variable is decomposed in the form of a normal mode

$$\tilde{q}(x, y, t) = \exp(\sigma t)\hat{q}(x, y), \tag{A 6}$$

where $\{\sigma, \hat{q}\}$ is a global mode that satisfies the generalized eigenvalue problem (2.3). It is written in a symbolic form

$$\mathbf{P}(\{\sigma, \hat{q}\}, Q) = \mathbf{0} \tag{A 7}$$

in which the dependence of the perturbation problem on the base flow Q explicitly appears. For convenience, in the derivation of the adjoint equations, the formal notation $\mathbf{P}(\{\sigma, \hat{q}\}, Q)$ is developed in a matrix form as

$$\mathbf{P}(\{\sigma, \hat{q}\}, Q) = \sigma \mathbf{B} \cdot \hat{q} + \mathbf{A}_0 \cdot \hat{q} + \mathbf{A}_1 \cdot \partial_x \hat{q} + \mathbf{A}_2 \cdot \partial_y \hat{q} - Re^{-1}\mathbf{B} \cdot (\partial_{x^2}\hat{q} + \partial_{y^2}\hat{q}), \tag{A 8}$$

where the derivation vectors are defined by $\partial_x \hat{q} = (\partial_x \hat{u}, \partial_x \hat{p})^T$, $\partial_y \hat{q} = (\partial_y \hat{u}, \partial_y \hat{p})^T$, $\partial_{x^2}\hat{q} = (\partial_{x^2}\hat{u}, \partial_{x^2}\hat{p})^T$, $\partial_{y^2}\hat{q} = (\partial_{y^2}\hat{u}, \partial_{y^2}\hat{p})^T$, and the matrices $\mathbf{B}, \mathbf{A}_0, \mathbf{A}_1$ and $\mathbf{A}_2$ by

$$\mathbf{B} = \begin{pmatrix} 1 & 0 & 0 \\ 0 & 1 & 0 \\ 0 & 0 & 0 \end{pmatrix}, \quad \mathbf{A}_0 = \begin{pmatrix} \partial_x U & \partial_y U & 0 \\ \partial_x V & \partial_y V & 0 \\ 0 & 0 & 0 \end{pmatrix},$$

$$\mathbf{A}_1 = \begin{pmatrix} U & 0 & 1 \\ 0 & U & 0 \\ 1 & 0 & 0 \end{pmatrix}, \quad \mathbf{A}_2 = \begin{pmatrix} V & 0 & 0 \\ 0 & V & 1 \\ 0 & 1 & 0 \end{pmatrix}.$$

Note that the matrices A_0, A_1 and A_2 depend on the base-flow variable Q and for that reason are real matrices. The boundary conditions for the global mode are

$$\hat{u} = 0 \quad \text{at the inlet and on the solid walls,} \tag{A 9}$$

$$(\partial_y \hat{u}, \hat{v}) = (0, 0) \quad \text{on the horizontal lateral boundaries,} \tag{A 10}$$

$$\hat{p}\, n - Re^{-1} (\nabla \hat{u}) \cdot n = 0 \quad \text{at the outlet.} \tag{A 11}$$

A.1.2. *Derivation of the gradient*

Variations of an eigenvalue σ with respect to the variation of the steady force F are investigated by looking for the sensitivity function $\nabla_\mathbf{F}\sigma$, defined as the gradient of the eigenvalue with respect to this forcing. In this Appendix it is rewritten as the gradient of the eigenvalue with respect to the control variable Q_F and denoted $\nabla_{Q_F}\sigma = (\nabla_\mathbf{F}\sigma, 0)^T$ The method used in this paper to determine this gradient is based on the introduction of Lagrange multipliers $Q^+ = (U^+, P^+)^T$ and $\hat{q}^+ = (\hat{u}^+, \hat{p}^+)^T$ to enforce, respectively, the constraint (A 1) between the base-flow variable and the control variable, and the constraint (A 7) between the perturbation and base-flow variable. Considering the inner product introduced in §2.1, a Lagrangian functional is defined as

$$L(Q, \sigma, \hat{q}, Q_F, Q^+, \hat{q}^+) = \sigma - \left(\hat{q}^+, \mathbf{P}(\{\sigma, \hat{q}\}, Q) \right) - \left(Q^+, \mathbf{B}F(Q) - Q_F \right). \tag{A 12}$$

The complex Lagrange multipliers Q^+ and $\hat{q}^+$ are referred to as the complex adjoint variables, respectively the adjoint base flow and the adjoint perturbation. Note that the state variable $(Q, \sigma, \hat{q})$, the control variable Q_F and the adjoint variable $(Q^+, \hat{q}^+)$ in the Lagrangian functional are now independent of each other. To determine the sensitivity function, the gradients of the Lagrangian with respect to these three variables are determined. The gradient with respect to the variable a is defined as

$$\frac{\partial L}{\partial a} \delta a = \lim_{s \to 0} \frac{L(a + s\delta a) - L(a)}{s}. \tag{A 13}$$

Cancelling the gradient with respect to the Lagrange multipliers $(Q^+, \hat{q}^+)$ leads to imposing the base-flow and perturbation equations, (A 1) and (A 7) respectively.

The adjoint equations and associated boundary conditions are obtained by considering the gradient of the Lagrangian with respect to the state variable $(Q, \sigma, \hat{q})$. According to the definition (A 13), this gradient is formally given by the sum of three terms:

$$\underbrace{- \left(\hat{q}^+, \mathbf{P}(\{\sigma, \hat{q}\}, \delta Q) \right) - \left(Q^+, \mathbf{B}FL(Q) \cdot \delta Q \right)}_{(a)}$$

$$+ \underbrace{\delta\sigma - \left(\hat{q}^+, \mathbf{P}(\{\delta\sigma, \hat{q}\}, Q) \right)}_{(b)} - \underbrace{\left(\hat{q}^+, \mathbf{P}(\{\sigma, \delta\hat{q}\}, Q) \right)}_{(c)} \tag{A 14}$$

where the formal notation $\mathbf{B}FL(Q) \cdot \delta Q$ arises from the linearization of the base-flow equations (2.2) around the base-flow state Q. It is equal to the homogeneous operator defined in equations (2.12).

Let us first consider the term labelled (c) in equation (A 14). Using the relations (A 7) and (A 8) and integrating by parts to remove the derivatives from the state

variables yields

$$(c) = \left(-\sigma^* \boldsymbol{B}_p \cdot \hat{\boldsymbol{q}}^+ - \boldsymbol{A}_0^T \cdot \hat{\boldsymbol{q}}^+ + \boldsymbol{A}_1 \cdot \partial_x \hat{\boldsymbol{q}}^+ + \boldsymbol{A}_2 \cdot \partial_y \hat{\boldsymbol{q}}^+ + Re^{-1} \boldsymbol{B} \cdot (\partial_{x^2} \hat{\boldsymbol{q}}^+ + \partial_{y^2} \hat{\boldsymbol{q}}^+), \delta \hat{\boldsymbol{q}}\right)$$

$$+ \text{boundary terms}, \quad (A\,15)$$

where the boundary terms appear due to the integration by parts. Eliminating the first term on the right-hand side of (A 15) leads to the definition of the adjoint perturbation equations

$$-\sigma^* \boldsymbol{B}_p \cdot \hat{\boldsymbol{q}}^+ - \boldsymbol{A}_0^T \cdot \hat{\boldsymbol{q}}^+ + \boldsymbol{A}_1 \cdot \partial_x \hat{\boldsymbol{q}}^+ + \boldsymbol{A}_2 \cdot \partial_y \hat{\boldsymbol{q}}^+ + Re^{-1} \boldsymbol{B} \cdot (\partial_{x^2} \hat{\boldsymbol{q}}^+ + \partial_{y^2} \hat{\boldsymbol{q}}^+) = \boldsymbol{0}. \quad (A\,16)$$

By eliminating the boundary terms in (A 15), the following boundary conditions are obtained:

$$\hat{\boldsymbol{u}}^+ = \boldsymbol{0} \text{ at the inlet and on the solid walls}, \quad (A\,17)$$

$$(\partial_y \hat{u}^+, \hat{v}^+) = (0, 0) \text{ on the horizontal lateral boundaries}, \quad (A\,18)$$

$$\hat{p}^+ \, \boldsymbol{n} - Re^{-1} (\nabla \hat{u}^+) \cdot \boldsymbol{n} = (\boldsymbol{U} \cdot \boldsymbol{n}) \hat{u}^+ \text{ at the outlet}. \quad (A\,19)$$

These define the boundary conditions of the adjoint perturbation problem.

Eliminating term (b) in the gradient (A 14) yields a normalization condition for the adjoint perturbation variable

$$\left(\hat{\boldsymbol{q}}^+, \boldsymbol{B} \cdot \hat{\boldsymbol{q}}\right) = 1. \quad (A\,20)$$

We now consider term (a) in the gradient (A 14) which leads to the definition of the adjoint base-flow equations. This term is composed of two sub-terms $(a)'$ and $(a)''$ which are defined as follows:

$$-\underbrace{\left(\hat{\boldsymbol{q}}^+, \mathbf{P}(\{\sigma, \hat{\boldsymbol{q}}\}, \delta \boldsymbol{Q})\right)}_{(a)'} - \underbrace{\left(\boldsymbol{Q}^+, \mathbf{BFL}(\boldsymbol{Q}) \cdot \delta \boldsymbol{Q}\right)}_{(a)''}. \quad (A\,21)$$

Rewriting term $(a)'$ in such a way that the base-flow state and its derivatives appear explicitly, we obtain

$$(a)' = \left(\hat{\boldsymbol{q}}^+, \boldsymbol{A}_0' \cdot \delta \boldsymbol{Q} + \boldsymbol{A}_1' \cdot \partial_x \delta \boldsymbol{Q} + \boldsymbol{A}_2' \cdot \partial_y \delta \boldsymbol{Q}\right), \quad (A\,22)$$

where the matrices $\boldsymbol{A}_0'$, $\boldsymbol{A}_1'$ and $\boldsymbol{A}_2'$ are defined by

$$\boldsymbol{A}_0' = \begin{pmatrix} \partial_x \hat{u} & \partial_y \hat{u} & 0 \\ \partial_x \hat{v} & \partial_y \hat{v} & 0 \\ 0 & 0 & 0 \end{pmatrix}, \quad \boldsymbol{A}_1' = \begin{pmatrix} \hat{u} & 0 & 0 \\ 0 & \hat{u} & 0 \\ 0 & 0 & 0 \end{pmatrix}, \quad \boldsymbol{A}_2' = \begin{pmatrix} \hat{v} & 0 & 0 \\ 0 & \hat{v} & 0 \\ 0 & 0 & 0 \end{pmatrix}.$$

Derivative terms on the right-hand side of equation (A 22) are integrated by parts. By doing this, boundary terms appear which are zero because only base-flow variations inside the computational domain are considered, i.e. $\delta \boldsymbol{Q} = 0$ at the inlet and the solid walls. After integration by parts and use of the incompressibility condition, we are left with

$$(a)' = \left(\boldsymbol{A}_0'^H \cdot \hat{\boldsymbol{q}}^+ - \boldsymbol{A}_1'^H \cdot \partial_x \hat{\boldsymbol{q}}^+ - \boldsymbol{A}_2'^H \cdot \partial_y \hat{\boldsymbol{q}}^+, \delta \boldsymbol{Q}\right). \quad (A\,23)$$

The term labelled $(a)''$ in equation (A 21) is now considered. We first rewrite $\mathbf{BFL}(\boldsymbol{Q}) \cdot \delta \boldsymbol{Q}$ in a convenient form:

$$\mathbf{BFL}(\boldsymbol{Q}) \cdot \delta \boldsymbol{Q} = \boldsymbol{A}_0 \cdot \delta \boldsymbol{Q} + \boldsymbol{A}_1 \cdot \partial_x \delta \boldsymbol{Q} + \boldsymbol{A}_2 \cdot \partial_y \delta \boldsymbol{Q} - Re^{-1} \boldsymbol{B} \cdot (\partial_{x^2} \delta \boldsymbol{Q} + \partial_{y^2} \delta \boldsymbol{Q}). \quad (A\,24)$$

Introducing (A 24) in $(a)''$ and integrating the derivative terms by parts yields:

$$(a)'' = \left(\boldsymbol{A}_0^T \cdot \boldsymbol{Q}^+ - \boldsymbol{A}_1 \cdot \partial_x \boldsymbol{Q}^+ - \boldsymbol{A}_2 \cdot \partial_y \boldsymbol{Q}^+ - Re^{-1}\boldsymbol{B} \cdot (\partial_{x^2} \boldsymbol{Q}^+ + \partial_{y^2} \boldsymbol{Q}^+), \delta \boldsymbol{Q}\right)$$

$$+ \text{ boundary terms.} \quad (A\,25)$$

Collecting the terms in expressions (A 23) and (A 25) and equating them to zero yields the definition of the adjoint base-flow equations:

$$\boldsymbol{A}_0^T \cdot \boldsymbol{Q}^+ - \boldsymbol{A}_1 \cdot \partial_x \boldsymbol{Q}^+ - \boldsymbol{A}_2 \cdot \partial_y \boldsymbol{Q}^+ - Re^{-1}\boldsymbol{B} \cdot (\partial_{x^2} \boldsymbol{Q}^+ + \partial_{y^2} \boldsymbol{Q}^+)$$
$$= -\boldsymbol{A}_0'^H \cdot \hat{\boldsymbol{q}}^+ + \boldsymbol{A}_1'^H \cdot \partial_x \hat{\boldsymbol{q}}^+ + \boldsymbol{A}_2'^H \cdot \partial_y \hat{\boldsymbol{q}}^+ \quad (A\,26)$$

associated with the adjoint base-flow boundary conditions:

$$\boldsymbol{U}^+ = \boldsymbol{0} \text{ at the inlet and on the solid walls,} \quad (A\,27)$$

$$(\partial_y \boldsymbol{U}^+, \boldsymbol{V}^+) = (0, 0) \quad \text{on the horizontal lateral boundaries,} \quad (A\,28)$$

$$\boldsymbol{P}^+\boldsymbol{n} + Re^{-1}(\nabla\boldsymbol{U}^+)\cdot\boldsymbol{n} = -(\boldsymbol{U}\cdot\boldsymbol{n})\boldsymbol{U}^+ + (\hat{\boldsymbol{u}}^*\cdot\boldsymbol{n})\hat{\boldsymbol{u}}^+ \text{ at the outlet.} \quad (A\,29)$$

Finally the gradient of the Lagrangian with respect to the steady force $\boldsymbol{Q}_F$ is given by

$$\frac{\partial L}{\partial \boldsymbol{Q}_F}\delta\boldsymbol{Q}_F = (\boldsymbol{Q}^+, \delta\boldsymbol{Q}_F). \quad (A\,30)$$

Noting that

$$\frac{\partial L}{\partial \boldsymbol{Q}_F}\delta\boldsymbol{Q}_F = (\nabla_{\boldsymbol{Q}_F}\sigma, \delta\boldsymbol{Q}_F) \quad (A\,31)$$

we see that the complex sensitivity function $\nabla_F\sigma$ is given by knowledge of the adjoint base-flow fields $\boldsymbol{U}^+$, according to

$$\nabla_F\sigma = \boldsymbol{U}^+. \quad (A\,32)$$

A.2. *Sensitivity to base-flow modifications*

The difference with the analysis detailed in §A1, is that the state is defined by the perturbation variable $\{\sigma, \hat{\boldsymbol{q}}\}$ and the control variable is now the base flow $\boldsymbol{Q}$. The sensitivity to base-flow modification is defined as the gradient of the eigenvalue with respect to this control variable, i.e. $\nabla_{\boldsymbol{Q}}\sigma = (\nabla_{\boldsymbol{U}}\sigma, \nabla_P\sigma)^T$. The same Lagrangian technique is used to determine the expression for this gradient. The state being constrained by the perturbation equation (A 7), only the Lagrange multiplier $\hat{\boldsymbol{q}}^+$ is introduced and the Lagrangian is now defined by

$$L(\boldsymbol{Q}, \sigma, \hat{\boldsymbol{q}}, \hat{\boldsymbol{q}}^+) = \sigma - \left(\hat{\boldsymbol{q}}^+, \mathbf{P}(\{\sigma, \hat{\boldsymbol{q}}\}, \boldsymbol{Q})\right). \quad (A\,33)$$

The gradients of the Lagrangian (A 33) with respect to the adjoint perturbation $\hat{\boldsymbol{q}}^+$ and the perturbation $\{\sigma, \hat{\boldsymbol{q}}\}$ are the same as in the analysis developed in §A1. Cancelling them then gives the perturbation equation and the adjoint perturbation equations. The gradient of the Lagrangian with respect to the base flow $\boldsymbol{Q}$ reduces to the opposite of term $(a)'$ of equation (A 21). According to (A 22), it may be written

$$\frac{\partial L}{\partial \boldsymbol{Q}}\delta\boldsymbol{Q} = -(\hat{\boldsymbol{q}}^+, \boldsymbol{A}_0'\cdot\delta\boldsymbol{Q} + \boldsymbol{A}_1'\cdot\partial_x\delta\boldsymbol{Q} + \boldsymbol{A}_2'\cdot\partial_y\delta\boldsymbol{Q}), \quad (A\,34)$$

In this formulation we can distinguish between modifications of the transport and production of perturbations due to the base-flow modifications δQ. The term $A'_0 \cdot \delta Q$ represents the modification of the transport operator, whereas the terms $A'_1 \cdot \partial_x \delta Q + A'_2 \cdot \partial_y Q$ represent the modification of the production operator. As seen in the previous section, successive integrations by parts leads to

$$\frac{\partial L}{\partial Q} \delta Q = (-A'^H_0 \cdot \hat{q}^+ + A'^H_1 \cdot \partial_x \hat{q}^+ + A'^H_2 \cdot \partial_y \hat{q}^+, \delta Q), \tag{A 35}$$

which yields the gradient of the eigenvalue σ with respect to the control variable Q:

$$\nabla_Q \sigma = -A'^H_0 \cdot \hat{q}^+ + A'^H_1 \cdot \partial_x \hat{q}^+ + A'^H_2 \cdot \partial_y \hat{q}^+. \tag{A 36}$$

It is clear that the term $-A'^H_0 \cdot \hat{q}^+$ arises from the modification of the transport operator whereas the terms $A'^H_1 \cdot \partial_x \hat{q}^+ + A'^H_2 \cdot \partial_y \hat{q}^+$ arise from the modification of the production operator. As a consequence, we obtain for the sensitivity to base-flow modifications, the following expression:

$$\nabla_U \sigma = -(\nabla \hat{u})^H \cdot \hat{u}^+ + \nabla \hat{u}^+ \cdot \hat{u}^*. \tag{A 37}$$

The first term is interpreted as the sensitivity to modifications of the transport of the perturbation by the base flow, and the second term as the sensitivity to modifications of the production of perturbations by the base flow.

Appendix B. Influence of non linearities on the eigenvalue variations

The sensitivity analysis is fundamentally linear since it is based on the evaluation of a gradient. In particular, base-flow modifications resulting from a steady force are sought as linear base-flow modifications. Therefore, a variation of the eigenvalue computed using the sensitivity analysis is exact in the limit of a force of small amplitude, but it only consists of a linear estimation for a force of unit order of magnitude.

To assess how nonlinearities alter the results obtained by the sensitivity analysis, a force of increasing amplitude, denoted $\delta F(\alpha)$, is placed at the station (x_0, y_0). We consider the model force given by equation (5.1) and increase its amplitude $\alpha ||U_0||^2$ through the coefficient α. For each value α, a linear estimation of the growth rate of the global mode pertaining to the forced base flow may be obtained using the sensitivity analysis to a steady force applied on the unforced base flow (see equation (5.2)). For this, the sensitivity analysis gives a linear estimation of the growth rate variation $\delta \lambda(\alpha)$ which, added to the growth rate of the unforced base flow denoted $\lambda(0)$, yields a linear estimation of the growth rate of the forced base flow, denoted $\lambda(0) + \delta \lambda(\alpha)$. This growth rate may also be evaluated exactly. To do this, the forced base flow is computed by solving the nonlinear base-flow equations (2.2) for the same amplitude α of the force. Solving the stability equations (2.3) and determining the leading eigenvalue gives the growth rate of the global mode of the forced base flow, denoted $\lambda(\alpha)$. The same procedure is applied to the global frequency to evaluate $\omega(0) + \delta \omega(\alpha)$ and $\omega(\alpha)$.

Results are shown in figure 15 for the Reynolds number $Re = 50$. On the left (resp. right) plots, the growth rate (resp. frequency) is depicted as a function of the amplitude of the force $\alpha ||U_0||^2$. The pairs of figures (a, b) and (c, d) show the results obtained for a force located at, respectively, the stations $(x_0 = 1.2, y_0 = 1.0)$ and $(x_0 = 1.2, y_0 = 2.0)$. The open circles show the results of the linear estimation whereas the filled circles show the exact nonlinear results obtained through the stability analysis of the forced
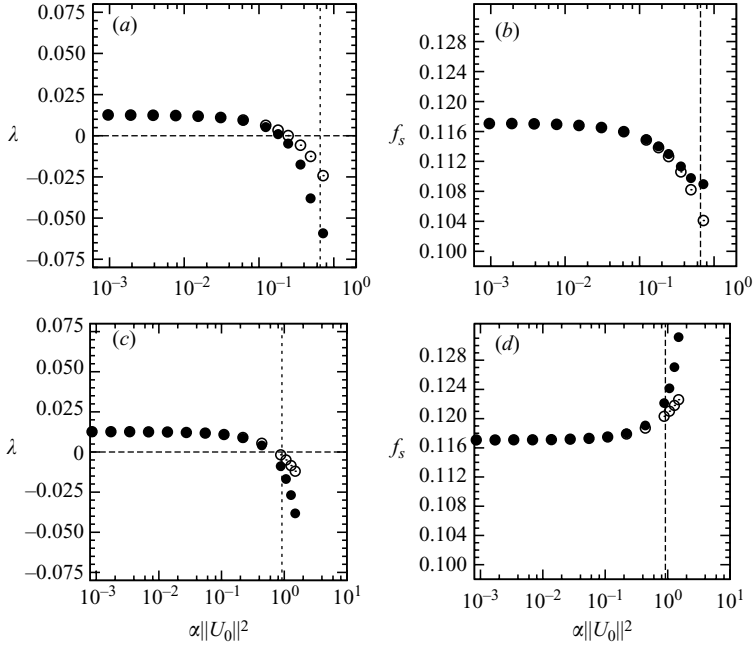
FIGURE 15. Growth rate λ (a, c) and global frequency $f_s = \omega/2\pi$ (b, d) as a function of the amplitude $\alpha\|U_0\|^2$ of a local steady force modelled by (5.1). The location of the force is (a, b) ($x_0 = 1.2$, $y_0 = 1.0$) and (c, d) ($x_0 = 1.2$, $y_0 = 2.0$). Comparison of the linear results obtained from the sensitivity analysis of the unforced base flow ($\circ$) with the nonlinear results obtained from the stability analysis of the forced base flow ($\bullet$), for $Re = 50$.

base. The vertical dashed line indicates the amplitude of the steady force (5.4) which models a control cylinder of diameter $d = 0.1$. For small amplitudes of the force $\alpha \ll 1$, the open and filled circles are superposed in all the figures since the base-flow modifications due to the force are linear in this case. This result validates the sensitivity analysis to a steady force, and in particular the accuracy of the sensitivity function. For the growth rate (see figure 15a, c), the linear prediction matches the growth rate of the forced base flow for values of the amplitude less than $\alpha\|U_0\|^2 \sim 0.2$. For larger amplitudes, and in particular, for the amplitude of the force which models a control cylinder of diameter $d = 0.1$, we observe a discrepancy, indicating that nonlinearities affect the global growth rate. For the two positions tested, the growth rate of the forced base flow is smaller than that predicted by the sensitivity analysis. Therefore the linear and nonlinear mechanisms have a cooperative action on the variation of the global growth rate. The true nonlinear stabilizing effect of the force is thus larger than that estimated by the sensitivity analysis. If we assume that this tendency is valid for other stations, we expect the extent of the stabilizing region to be larger in the experiments than in the theoretical analysis. A comparison of figures 10 and 12 confirms this tendency, but only for Reynolds numbers $Re \geqslant 55$. On the contrary, for Reynolds numbers close to the critical Reynolds number ($Re = 48$ and 50), the experimental stabilizing region is smaller than the predicted one. Therefore nonlinearities cannot be invoked to explain the discrepancies between the experimental and predicted results.

For the frequency (see figure 15b, d), we observe that the linear estimation is valid up to $\alpha\|U_0\|^2 \approx 0.2$. The frequency is decreased when the force is located at the station ($x_0 = 1.2$, $y_0 = 1.0$) (figure 15b) and increased when placed at ($x_0 = 1.2$, $y_0 = 2.0$)
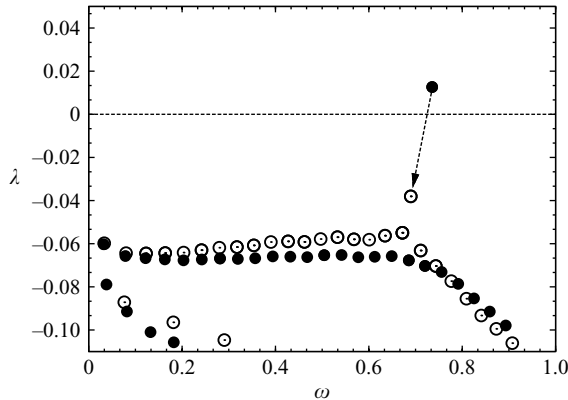
FIGURE 16. Comparison of the spectrum obtained for the unforced base flow (filled circles) and the forced base flow (open circles). The leading global mode is shifted from the unstable half-plane ($\lambda > 0$) to the stable half-plane ($\lambda < 0$), as shown by the arrow, whereas the stable global modes remain in the stable half-plane. Amplitude and location of the steady force: $\alpha ||U_0||^2 = \dots$; ($x_0 = 1.2$, $y_0 = 1.0$). $Re = 50$.

(figure 15d). This is in agreement with results plotted in figure 11(b). For $\alpha ||U_0||^2 \geqslant 0.2$, nonlinear mechanisms alter the linear estimation of the frequency. Their effect depends on the location of the force. For the station ($x_0 = 1.2$, $y_0 = 1.0$), the linear and nonlinear mechanisms have opposite trends, since the true nonlinear global frequency of the forced base flow is reduced less than the linear estimation. On the other hand, for the station ($x_0 = 1.2$, $y_0 = 2.0$), they cooperate since the true global frequency is increased more than the linear estimation. The effect of nonlinearities on the frequency seems to be more complex than on the growth rate variations.

Appendix C. Are the stable global modes destabilized by the force?

Throughout this paper, we claim that the flow is stabilized by a local steady force if the most unstable global mode of the unforced base flow is stabilized. This is true only if the stable modes are not destabilized by the local force. To verify this, we compute the spectrum of the base flow forced at the station ($x_0 = 1.2$, $y_0 = 1.0$). Figure 16 depicts this spectrum (open circles) and, for comparison, the spectrum of the unforced base flow (filled circles). As expected, the most unstable global eigenvalue is shifted in the stable half-plane ($\lambda < 0$) under the action of the force (see the arrow in the figure). The stable global eigenvalues are only slightly shifted and remain in the stable half-plane. This shows that the flow is stabilized by the local steady force.

REFERENCES

AIRIAU, C., BOTTARO, A., WALTHER, S. & LEGENDRE, D. 2003 A methodology for optimal laminar flow control: Application to the damping of Tollmien-Schlichting waves in a boundary layer. *Phys. Fluids* **15**, 1131–1145.

BARKLEY, D. 2006 Linear analysis of the cylinder wake mean flow. *Eurphys. Lett.* **75**, 750–756.

BOTTARO, A., CORBETT, P. & LUCHINI, P. 2003 The effect of base flow variation on flow stability. *J. Fluid Mech.* **476**, 293–302.

CHOMAZ, J. M. 2005 Global instabilities in spatially developing flows: non-normality and nonlinearity. *Annu. Rev. Fluid Mech.* **37**, 357–392.

CHOMAZ, J.-M., HUERRE, P. & REDEKOPP, L. G. 1988 Bifurcations to local and global modes in spatially developing flows. *Phys. Rev. Lett.* **60**, 25–28.

CHOMAZ, J.-M., HUERRE, P. & REDEKOPP, L. G. 1991 A frequency selection criterion in spatially developing flows. *Stud. App. Maths* **84**, 119–144.

DAVIS, T. A. 2004 A column pre-ordering strategy for the unsymmetric-pattern multifrontal method. *ACM Transactions on Methematical Software* **30** (2), 165–195.

DAVIS, T. A. & DUFF, I. S. 1997 An unsymmetric-pattern multifrontal method for sparse lu factorization. *SIAM J. Matrix Anal. Applics.* **18**, 140–158.

GIANNETTI, F. & LUCHINI, P. 2007 Structural sensitivity of the cylinder wake's first instability. *J. Fluid Mech.* **581**, 167–197.

GUNZBURGER, M. D. 2007 Inverse design and optimization methods. *Von Karman Institute for Fluid Dynamics Lecture Series* 1997-05.

HILL, D. C. 1992 A theoretical approach for analysing the restabilization of wakes. *AIAA* 92-0067.

HUERRE, P. & MONKEWITZ, P. A. 1990 Local and global instabilites in spatially developing flows. *Annu. Rev. Fluid Mech.* **22**, 473–537.

HWANG, Y. & CHOI, H. 2006 Control of absolute instability by basic-flow modification in parallel wake at low Reynolds number. *J. Fluid Mech.* **560**, 465–475.

JACKSON, C. P. 1987 A finite-element study of the onset of vortex shedding in flow past variously shaped bodies. *J. Fluid Mech.* **182**, 23–45.

KIM, H. B. & CHANG, K. S. 1995 Numerical study on vortex shedding from a circular cylinder influenced by a nearby control wire. *Comput. Fluid Dyn. J.* **4**, 151–164.

LEHOUCQ, R. B., SORENSEN, D. C. & YANG, C. 1998 *ARPACK Users's Guide*. SIAM, *Philadelphia*.

MATHIS, C., PROVANSAL, M. & BOYER, L. 1984 Benard-von Karman instability: an experimental study near the threshold. *J. Phys. Lett. Paris* **45**, 483–491.

MITTAL, S. & RAGHUVANSHI, A. 2001 Control of vortex shedding behind circular cylinder for flows at low Reynolds number. *Intl. J. Numer. Meth. Fluids* **35**, 421–447.

MONKEWITZ, P. A., HUERRE, P. & CHOMAZ, J.-M. 1993 Global linear stability analysis of weakly non-parallel shear flows. *J. Fluid Mech.* **251**, 1–20.

MORZYNSKI, M., AFANASIEV, K. & THIELE, F. 1999 Solution of the eigenvalue problems resulting from global non-parallel flow stability analysis. *Comput. Meth. Appl. Mech. Engng* **169**, 161–176.

NOACK, B. R. & ECKELMANN, H. 1994 A global stability analysis of the steady and periodic cylinder wake. *J. Fluid Mech.* **270**, 297–330.

PIER, B. 2002 On the frequency selection of finite-amplitude vortex shedding in the cylinder wake *J. Fluid Mech.* **458**, 407–417.

PROVANSAL, M., MATHIS, C. & BOYER, L. 1987 Bnart-von Karman instability: transient and forced regimes. *J. Fluid Mech.* **182**, 1–22.

SIPP, D. & LEBEDEV, A. 2007 Global stability of base- and mean-flows: a general approach and its applications to cylinder and open cavity flows. *J. Fluid Mech.* **593**, 333–358.

SORENSEN, D. C. 1992 Implicit application of polynomial filters in a k-step Arnoldi method. *SIAM J. Matrix Anal. Appl.* **13**, 357–385.

SREENIVASAN, K. R., STRYKOWSKI, P. J. & OLINGER, D. J. 1987 Hopf bifurcation, Landau equation, and vortex shedding behind circular cylinders. In *Proc. Forum on Unsteady Flow Separation.* (ed. K. Ghia), pp. 1–13. ASME

STRYKOWSKI, P. J. & SREENIVASAN, K. R. 1990 On the formation and suppression of vortex shedding at 'low' Reynolds numbers. *J. Fluid Mech.* **218**, 71–107.

WILLIAMSON, C. H. K. 1996 Vortex dynamics in the cylinder wake. *Annu. Rev. Fluid Mech.* **28**, 477–539.

ZEBIB, A. 1987 Stability of viscous flow past a circular cylinder *J. Engrg Maths* **21**, 155–165.